

Sequential star formation in a cometary globule (BRC37) of IC1396

Hisashi Ikeda,¹ Koji Sugitani,¹ Makoto Watanabe,² Naoya Fukuda,³ Motohide Tamura,⁴ Yasushi Nakajima,⁴ Andrew J. Pickles,⁵ Chie Nagashima,⁶ Takahiro Nagayama,⁷ Hidehiko Nakaya,² Makoto Nakano,⁸ and Tetsuya Nagata⁷

ABSTRACT

We have carried out near-IR/optical observations to examine star formation toward a bright-rimmed cometary globule (BRC37) facing the exciting star(s) of an HII region (IC1396) containing an IRAS source, which is considered to be an intermediate-mass protostar. With slitless spectroscopy we detected ten H α emission stars around the globule, six of which are near the tip of the globule and are aligned along the direction to the exciting stars. There is evidence that this alignment was originally toward an O9.5 star, but has evolved to align toward a younger O6 star when that formed. Near-IR and optical photometry suggests that four of these six stars are low-mass young stellar objects (YSOs) with masses of $\sim 0.4 M_{\odot}$. Their estimated ages of ~ 1 Myr indicate that they were formed at the tip in advance of the formation of the IRAS source. Therefore, it is likely that sequential star formation has been taking place along the direction from the exciting stars toward the IRAS source, due to the UV impact of the exciting star(s). Interestingly, one faint, H α emission star, which is the closest to the exciting star(s), seems to be a young brown dwarf that was formed by the UV impact in advance of the formation of other YSOs at the tip.

¹Graduate school of Natural Sciences, Nagoya City University, Mizuho-ku, Nagoya 467-8501, Japan

²Subaru Telescope, National Astronomical Observatory of Japan, Hilo, HI 96720

³Department of Computer Simulation, Okayama University of Science, 1-1 Ridai-cho, Okayama 700-0005, Japan

⁴National Astronomical Observatory, 2-21-1 Osawa, Mitaka, Tokyo 181-8588, Japan

⁵Las Cumbres Observatory, Goleta CA 93117

⁶Department of Astrophysics, Nagoya University, Chikusa-ku, Nagoya 464-8602, Japan

⁷Department of Astronomy, Kyoto University, Sakyo-ku, Kyoto 606-8502, Japan

⁸Faculty of Education and Welfare Science, Oita University, Oita 870-1192, Japan

Subject headings: ISM: cloud — ISM: globules — ISM: individual (IC1396) — stars: formation — stars: pre-main-sequence — stars: brown dwarf

1. Introduction

Small molecular clouds or globules are often seen as small dark patches in the peripheries of HII regions, having bright rims on the side facing the exciting stars of the HII regions. These bright-rimmed clouds (BRCs) /globules are considered to be pre-existing denser parts in the original molecular cloud that formed the HII region, or parts that became denser due to the expansion of the HII region. After evaporation of their thinner ambient molecular gas, they will be exposed directly to the UV radiation from the exciting stars, forming ionization fronts (bright rims) on the exciting star sides. Because of the high pressure of the bright rim and the geometrical focusing, molecular gas could be squeezed and consequently has a higher density to form stars (e.g., Sandford et al. 1982; Bertoldi 1989; Lefloch & Lazareff 1994; Williams et al. 2001; Kessel & Burkert 2003; Miao et al. 2006; Motoyama et al. 2007). Therefore, BRCs are potential sites of induced star formation due to compression by ionization/shock fronts.

In fact, many signposts of star formation, i.e., IRAS point sources, molecular outflows, HH objects, reflection nebulae, and so on, have been reported in BRCs (e.g., Table 1 of Elmegreen 1998). Our systematic near-IR imaging of the IRAS-associated BRCs of Sugitani et al. (1991) revealed that many of them are associated with small young clusters or aggregations, some of which have asymmetric distributions biased toward the exciting-star side along the axes of BRCs. This indicates that these young stars formed prior to the formation of the IRAS sources (protostar-like objects), i.e., propagation of star formation along the axis of BRC as the ionization/shock front advances outward of the HII region (Sugitani et al. 1995). Recently, this sequential star formation was more clearly confirmed in BRC14 (SFO14; Matsuyanagi et al. 2006) and BRC38 (SFO38; Getman et al. 2007), and the precursor of such star formation was reported in BRC75 (SFO75; Urquhart et al. 2007).

Three-dimensional (3D) simulations imply that some radiationally imploded globule repeat leaving small cores decoupled from itself, which collapse after passage of the ionization/shock front and form stars, i.e., sequential star formation in the globule (Kessel & Burkert 2003).

BRC37 (SFO37) is a small cometary globule with a bright rim in the southern periphery of IC1396 ($d \sim 750$ pc; Matthews 1979). It is located ~ 12 pc from the main exciting star

(HD206267, O6) and the size of this globule is $\sim 0'.6$ wide and $\sim 3'$ long in the optical (Fig. 1). IRAS 21388+5622 ($L \sim 155L_{\odot}$) is located at the tip of the globule. It is considered to be an A star (Schwartz et al. 1993) having a molecular outflow with a dynamical age of ~ 0.3 Myr (Duvert et al. 1990). Recently, Morgan et al. (2008) reported that the luminosity of the internal source of this globule was estimated to be $63L_{\odot}$, corresponding to a spectral type of B9.

Our interferometric ^{13}CO observations clearly showed two tails of blueshifted velocities that stretch from the globule tip away from the main exciting star (Sugitani et al. 1997). This suggests a UV impact from the exciting star of IC1396 and a velocity pattern that may be explained by the collapsing inward gas motion (e.g., Lefloch & Lazareff 1994).

Near-IR imaging revealed that several low-mass young stellar object (YSO) candidates were located at the globule tip facing the exciting star (Sugitani et al. 1995). These near-IR sources are nearly aligned along the globule axis (Sugitani et al. 1997, 1999) and this object is considered to be a representative of the sequential star formation in BRCs. Some of them were identified as $\text{H}\alpha$ emission stars, which are most likely to be T Tauri stars (Ogura, Sugitani & Pickles 2002, hereafter OSP), supporting the concept of sequential star formation. However, the details of the star formation were not clear from previous observations. Since the masses and ages of the YSO candidates were still unknown, we could not previously establish the sequence of star formation or its time scale.

In order to estimate the masses and ages of the YSO candidates, we have now confirmed their $\text{H}\alpha$ emissions with slitless spectroscopy and carried out additional optical and near-IR photometry. Here we present our spectroscopic and photometric results and discuss sequential star formation in BRC37. Additionally, we show our narrowband imaging of the $v=1-0$ S(1) H_2 line to examine star formation activity of the YSO candidates.

Finally we discuss the candidate closest to the exciting stars, which seems from our photometric analysis to be a very low-mass object, i.e., a young brown dwarf candidate. Since sequential star formation from the direction of the exciting stars to the opposite side is suggested for BRC37, this outermost candidate was likely formed by UV impact prior to the formation of other YSO candidates, and represents the first observational evidence for brown dwarf formation as a consequence of UV impact.

2. Observations

2.1. Optical observations

Slit-less grism spectroscopy and g' (482.5nm), i' (767.2nm), and wide H α (651nm) imaging of BRC37 were conducted on 2006 November 19 UT and V , and I_C imaging was done on 2007 August 7 UT with the Wide Field Grism Spectrograph 2 (WFGS2; Uehara et al. 2004) mounted on the University of Hawaii 2.2-m telescope (UH88). The detector used was a Tektronix 2048×2048 CCD. The pixel scale is $0''.34 \text{ pixel}^{-1}$, yielding a field of view of $11.5' \times 11.5'$. For the slitless spectroscopy, we used a wide H α filter (FWHM = 50nm) and a 300 line mm^{-1} grism, providing a dispersion of $3.8 \text{ \AA pixel}^{-1}$.

Three 120 s exposures dithered by $10''$ and single 60 s and 30 s exposures were taken at wide H α , g' and i' , respectively. For the slitless spectroscopy, we took three 300 s exposures dithered by $10''$. The seeing was $\sim 0''.8$ (FWHM) in the wide H α image. For the photometric calibration the SDSS standard star BD +38 $^\circ$ 4955 (Smith et al. 2002) was observed at nearly the same airmass as the target (difference $\lesssim 0.02$). Twilight images were taken for flat-fielding. The limiting magnitudes at 0.1 mag error level were ~ 21.6 at g' and ~ 20.4 at i' .

Three 60 s and three 30 s exposures dithered by $10''$ were taken at the V and I_C bands, respectively. The seeing was $\sim 1''.0$ (FWHM) in the V band. For the photometric calibration, the Landolt standard star (Landolt 1992) was observed at nearly the same airmass as the target (difference $\lesssim 0.02$). The limiting magnitudes at 0.1 mag error level were ~ 21.7 at V and ~ 19.8 at I_C .

2.2. Near-infrared observations

J ($1.25\mu\text{m}$), H ($1.63\mu\text{m}$), and K_s ($2.14\mu\text{m}$) band imaging of BRC37 was conducted on 2001 August 29 UT with SIRIUS (the Simultaneous three-color InfraRed Imager for Unbiased Survey; Nagashima et al. 1999; Nagayama et al. 2003) mounted on UH88. The SIRIUS camera, equipped with three 1024×1024 pixel HAWAII arrays, enables simultaneous observations in the J , H , and K_s bands. The pixel scale is $0''.288 \text{ pixel}^{-1}$, yielding a field of view of $4.9' \times 4.9'$. The region of the near-infrared observation is shown as a square in Fig.1.

We obtained thirty dithered frames with a 30 s exposure, resulting in a total exposure time of 900 s. The seeing was $\sim 1''.0$ (FWHM) in the K_s band. The limiting magnitudes at 0.1 mag error level were ~ 19.7 at J , ~ 18.7 at H , and ~ 18.0 at K_s . We observed P9107 of the faint near-infrared standard star catalog (Persson et al. 1998) for the photometric

calibration. Dome-flat frames were taken for flat-fielding.

Narrow-band imaging of H_2 + continuum ($2.12\mu\text{m}$) and continuum ($2.26\mu\text{m}$) was made on 1998 September 2 UT with QUIRC (the Quick Infrared Camera; Hodapp et al. 1996) mounted on UH88. The pixel scale is $0''.189 \text{ pixel}^{-1}$, yielding a field of view of $3.2' \times 3.2'$. We obtained ten frames of 150 s exposure dithered by $10''$, resulting in a total exposure time of 1500 s for the H_2 line. We also obtained ten dithered frames of 75 s exposure, resulting in a total exposure time of 750 s for the continuum. Dome-flat frames were taken for flat-fielding.

2.3. Data reductions

We have applied the standard procedures for optical/NIR image reduction with IRAF (bias/dark subtraction, flat-fielding and averaging of dithered images). The combined images of the wide $\text{H}\alpha$ and JHK_s bands are shown in Fig. 1 and 2, respectively.

We searched for $\text{H}\alpha$ emission stars in the combined image of slitless spectroscopy. For the detected candidates of the emission-line stars, we have made 1D spectra with the aperture extraction package of IRAF and measured their equivalent widths (EWs) with SPLOT.

Stellar sources were initially identified by DAOFIND with a 4σ detection threshold and all the photometric measurements were made with the DAOPHOT package. For the V and I_C band photometry, we made rough linear color-corrections from the observations of several standard stars (Landolt 1992), assuming average extinctions ($0.10 \text{ mag airmass}^{-1}$ at the V band and $0.08 \text{ mag airmass}^{-1}$ at the I_C band) of Mauna Kea¹. For the JHK_s magnitudes and colors, we made the color conversion from the UH88/SIRIUS system to the CIT system (Nagashima et al. 1999).

3. Results

3.1. Selections of YSO candidates

3.1.1. Optical selection : $\text{H}\alpha$ emission stars

We searched for $\text{H}\alpha$ emission stars as YSO candidates. We detected ten $\text{H}\alpha$ emission stars with slitless spectroscopy and refer to them as E1–E10 (Fig. 1). Six of them (E1–E6)

¹CFHT observatory Manual, Section 2
(http://www.cfht.hawaii.edu/Instruments/ObservatoryManual/CFHT_Observatory_Manual_TOC.html)

are located toward the tip of BRC37 (Fig. 3 left). The EWs of the ten H α emission stars are listed with their coordinates in Table 1. E2–E5 and E7–E9 are candidates for classical T Tauri stars (CTTS) with EW ≥ 10 Å. The continuum fluxes of E1, E6 and E10 are too faint to be measured, but these sources are also good candidates for classical T Tauri stars since their H α emission lines are rather strong compared with their continua. E6 has [SII] λ 6731, [NII] λ 6584, and [OI] λ 6300 emission lines (Fig. 3 left).

In the previous work (Ogura, Sugitani & Pickles 2002), the detection of eight H α emission stars was reported toward BRC37 (OSP 37-1 to -8; Fig. 3 right).

Six of these are confirmed here and cross referenced in Table 1. Additionally, as can be seen in Fig. 3, E4 is a strong H α emission source with weak continuum that is newly present in the 2006 observations. E4 is located just South of OSP 37-5. Its H α emission is clearly seen in the slitless spectroscopic image from 2006 (Fig. 3 left), whereas no counterpart is evident in the 1997 image (Fig. 3 right). Thus E4, as well as E7, E9 and E10 (which lie outside the 1997 image), are newly detected in these observations. E7 and E8 are located north of BRC37, and E9 and E10 south of BRC37, being not associated with the BRC37 globule (Fig. 1).

However we can not confirm two H α sources from 1997, which appear to have been misidentified in OSP. OSP 37-5 is the continuum source just to the North of E4. It was previously classified as a weak H α source, but closer examination of both the 2006 and 1997 data reveals that its spectrum has a saw-toothed ripple, with a peak near H α . The narrow peak head of this ripple might be confused with H α emission, but it is more likely an M star. This more careful analysis also reveals that OSP 37-4, to the East of E2, was also misclassified as an H α source, probably due to confusion with the overlapping continuum of E2.

We noticed that the EWs in Table 5 of Ogura, Sugitani & Pickles (2002) are smaller than those of this work, by about a factor of 3.8 on average. Accordingly we recalculated the EWs of the OSP stars from the 1997 data, using the improved methodology applied in this work. We confirmed that this discrepancy was due to the failure to scale from pixel to angstrom in OSP, and not to any large variation of H α emission. Table 1 lists the EWs measured in this work for BRC37 in column 4, and those corrected from the 1997 data in the last column.

The data presented in Table 5 of OSP were *not* scaled from pixel to angstrom, and the data presented there for BRC13 are a repetition of that for BRC12. Accordingly we show here in an appendix as Table 4 a fully corrected version of Table 5 from OSP, recalculated with our improved methodology, and properly scaled.

3.1.2. NIR selection : NIR excess sources

We show the $J - H$ vs. $H - K$ color-color diagram in Fig. 4. While E1 and E8 are below the T Tauri locus on the color-color diagram, E2–E7, E9, and E10 are located in the reddening zone of the T Tauri locus which indicates they are candidate classical T Tauri stars.

In order to select sources having large near-infrared excess as YSOs candidates, we searched for NIR sources that can be explained as classical T Tauri stars with large NIR excess or those with circumstellar envelope on the color-color diagram (Fig. 4). We also examine E1–E10, which are identified as YSO candidates here.

Since E7–E10 are outside of our NIR imaging area (Fig. 1), we referred to the 2MASS data and additionally plotted E8 in Fig. 4, after converting the 2MASS data to the CIT system (Carpenter 2001). We did not plot E7, E9 and E10; for E7 2MASS provides only upper limits at H and K_s and, while single sources are cataloged/identified toward E9 and E10 in the 2MASS catalog/images, our optical images show they have close stars with separations of $\lesssim 2.0''$, so their 2MASS colors are unreliable.

We included the sources located in the region surrounded by the reddening band of main-sequence stars and giants, the reddening line that originates from the truncated point of the T Tauri locus, and the T Tauri locus of Meyer et al. (1997) with the color-color diagram. We took photometric errors into account for this selection. We excluded sources whose color errors could possibly make them those without NIR excess. We included those redward of the reddening line from the truncated point. This results in a total of seven NIR sources selected here as YSO candidates. Two of them (the IRAS source and E6) have been identified as YSO candidates previously. We refer to the other five NIR excess sources as I1–I5 (Fig. 2). I1 and I2 are located toward the tip of BRC37, and I3 is located toward the tail of BRC37. I4 and I5 are located east of BRC37.

Several NIR-excess sources below the T Tauri locus (Fig. 4) are too faint ($J \gtrsim 16$) to be intermediate-mass YSOs associated with this region, suggesting that they are background stars. Two sources have the possibility that they are (young) substellar objects from the following analysis with another color-color diagram. One is E1 and the other is referred to here as I6 (Fig. 4).

In order to eliminate the possibility that these candidates could be galaxies, we use the $i' - J$ vs. $J - K$ color-color diagram (Fig. 5). We use the transform equation (Eq. 8 and Table 3) of Jordi et al. (2006) to obtain the i' magnitude of main-sequence stars and giants. We also compared this with our own transform equation obtained by observing several standard stars of Landolt (1992). We found the difference between i' magnitudes

calculated from these two methods to be small, $\lesssim 0.025$ mag. in a range of $0 \lesssim R - I \lesssim 2.2$, and therefore adopt the transformation of Jordi et al. (2006).

Galaxies lie blueward of the reddening band of main sequence stars and giants (e.g., Nagashima et al. 2003). From this diagram, I2 is judged to be a galaxy. I3 is located near the boundary of the reddening band. Our slitless spectroscopic image shows no H α emission for I3, suggesting that it is not a T Tauri star associated with the tail of BRC37. Taking into account its errors of color magnitude, it is also likely to be a galaxy. I4 and I5 are too faint to be measured in the i' band image and only 3σ upper limits is given. Although I4 can not be classified, the appearance of I5 on the JHK_s images suggests that I5 is a galaxy.

The position of I1 is $[\alpha(2000), \delta(2000)] = [21^{\text{h}}40^{\text{m}}27^{\text{s}}.94, +56^{\circ}36'02''.38]$. The color-color diagram can not be used for I1 since there is no detection at i' . However I1 has a large NIR excess and a NIR nebulosity (Fig. 2), and is most likely to be an embedded YSO inside BRC37.

Only E1 and I6 have the colors of late M-dwarfs or reddened late M-dwarf on the color-color diagram, leaving the possibility that these are (young) substellar objects.

3.1.3. NIR Selection : More Embedded Sources ?

In order to select embedded Class I candidates in BRC37 and its neighboring clouds (two small clouds south-west of BRC37, Fig. 2), we examined NIR sources that are detectable both at H and K_s , but not at J , and found seven such sources by this method. We further examined their association with molecular cloud cores. Baba et al. (2006) reported that most of protostar (Class I) candidates are associated with the C¹⁸O clumps distributed throughout the cloud C of the Vela Molecular Ridge by their deep NIR imaging. Here we consider the sources located toward the centers of cloud cores to be possible Class I candidates.

Following these selection criteria, we list three “red” NIR sources named R1–R3 (Fig. 2). R1 has an $H - K$ color magnitude of ~ 2.4 , which suggests a possibility that R1 is a Class I source embedded in the tail of BRC37. The position of R1 corresponds to the peak located at the $(45'', -56'')$ offset position in the ¹³CO ($J=1-0$) channel map of $V_{\text{LSR}} = 1.25$ km s⁻¹ (Fig. 4b of Duvert et al. 1990). R2 is $\sim 0.15'$ north of R1, near the $(45'', -56'')$ ¹³CO peak, and R3 is $\sim 0.76'$ north-northwest of R1, toward the center of the $(20'', -8'')$ ¹³CO peak. R2 and R3 have $H - K$ color magnitudes of $\sim 1.1-1.2$, which are similar to those of reddened T Tauri stars with near-IR excess (e.g., E6 in Fig. 4), but Baba et al. (2006) showed that some class I sources appear in the $J - H$ vs. $H - K$ diagram in the region of reddened T Tauri stars having NIR excess. Because R1–R3 are located toward CO intensity peaks, i.e.,

molecular clumps, all of them are possible Class I candidates.

3.1.4. H_2 ($v=1-0$, $S(1)$) emission-line

In order to examine star formation activities of the YSO candidates, we searched for H_2 emission around them. We show a false color image of H_2 emission and continuum in Fig. 6a.

Toward the immediate east-vicinity of the IRAS source, two lobes that extend from the IRAS source are shown. They probably correspond to the walls at the root of the cavity that was created by the outflow pointing to the NE2 knot of HH588 (P.A. $\sim 60^\circ$ from the IRAS source). A bow structure (Ia) can be identified $\sim 0'.7$ northeast of the IRAS source (P.A. $\sim 54^\circ$ from the IRAS source). This probably corresponds to the NE1 A and B knots of HH588. A counterpart (Ib) of this bow structure is also identified $\sim 0'.7$ southwest of the IRAS source (P.A. $\sim 220^\circ$ from the IRAS source). In addition, a partial, compact bow structure (IIa) is also identified $\sim 0'.4$ north-northeast of the IRAS source (P.A. $\sim 32^\circ$ from the IRAS source). A counterpart (IIb) of this compact bow structure is faintly identified $\sim 0'.4$ south-southwest of the IRAS source (P.A. $\sim 206^\circ$ from the IRAS source), while it is invisible in the optical. In Fig. 6b, we show the schematic drawing of these H_2 structures, which are considered to be geometrically related to the outflow activities of the IRAS source and thus are likely to be shock-excited.

3.2. Examination of YSO Candidates

Table. 2 shows the properties of the YSO candidates, which are derived from our photometry.

We examined the photometric variability at i' and g' for our detected $H\alpha$ emission stars by comparing another WFGS2 observation that was conducted on 2006 September 22. Although these stars showed small differences between the two epochs ($\lesssim 0.6$ mag), the variability is not clear due to their faintness and 3σ errors of ~ 0.1 – 0.3 mag in relative photometry.

We further compared the g' image with the V image (Fig. 7). The intensities of E2, E3, E5 and E6 in the g' and V images are similar, whereas E4 can not be identified on the V image (Fig. 7 left). Precise measurement of this variation is difficult due to contamination from a neighboring brighter star, but our rough estimate indicates that the magnitude difference is ~ 3 mag. or larger. A similar variation is also seen between the I_C and i' images.

Thus E4 may be a background, cataclysmic variable star with $H\alpha$ emission, although we cannot eliminate the possibility of occultation due to the circumstellar material of E4 (e.g., a precession disk, inhomogeneous disk structure, etc.). The variation of E4 is very rare, and follow-up observations are required to monitor it.

We also examined the variability of $H\alpha$ emission for the $H\alpha$ emission stars. The variability of the EWs for E2, E3, E5, and E8 is at several ten percent level over the 10 yr period (Table 1), and seems to be natural for CTTSs. As was mentioned in Section 3.1.1, the $H\alpha$ emission of E4 is identified in the spectroscopic image of this work, but not in that of the previous work from 1997. This again indicates very large variability of $H\alpha$ emission for E4.

For E6, [SII] λ 6731, [NII] λ 6584, and [OI] λ 6300 emission lines are seen in the spectroscopic image of this work, but not in that of the previous work (Fig. 3 right). This variation may indicate outflow variability of E6 or a clearance of its circumstellar material.

We can estimate the masses and ages of the five $H\alpha$ emission stars (E1–E3, E5, and E6) by assuming that they are classical T Tauri stars associated with IC1396 ($d=750$ pc). We made an extinction corrected color-magnitude diagram (i' vs. $i' - J$ diagram, Fig. 8) with the evolutionary tracks and isochrones of Palla & Stahler (1999). Additionally, we used $A_V=0.652A_V$ derived from Cardelli et al. (1989) for extinction correction. We adopted the T Tauri locus of Meyer et al. (1997) as the intrinsic colors of these emission stars, except for E1, and evaluate their extinctions on the $J - H$ vs. $H - K$ diagram by using the reddening law of Cohen et al. (1981). By this method we calculate that E2, E3, E5, and E6 have ages of ~ 1 Myr and masses of ~ 0.3 – $0.5 M_\odot$. We also constructed I_C vs. $I_C - J$ diagram and found slightly smaller masses (~ 0.2 – $0.4 M_\odot$). Since these masses and ages are typical for T Tauri stars, we conclude that E2, E3, E5, and E6 are very likely to be T Tauri stars.

We note that E4 is located below the 10 Myr isochrone on the i' vs. $i' - J$ diagram, suggesting that it is not a T Tauri star associated with IC1396.

It is difficult to evaluate the mass and age of E1 from the i' vs. $i' - J$ diagram with the evolutionary tracks and isochrones of Palla & Stahler (1999); its magnitude is very faint and its extinction cannot be estimated from its color-magnitude location, which is below the T Tauri locus on the $J - H$ vs. $H - K$ diagram (Fig. 4). Instead, we constructed J vs. $J - H$ color magnitude diagram (Fig. 9), adopting the isochrones of the NextGen model (Baraffe et al. 1998). The reddening line, which originates from a $0.075 M_\odot$ star of the 1.0 Myr locus, indicates the boundary between H-burning stars and brown dwarfs. In this diagram, E1 lies below this reddening line, suggesting that it is a young brown dwarf with $H\alpha$ emission. Even if the 3 Myr locus is adopted, E1 again falls below the reddening line from a $0.075 M_\odot$ star.

We estimated $A_V \sim 2.0$ for E1 with the 1 Myr locus in Fig. 9. Even with the 3Myr locus, the estimated value is the same. However, E1 could have NIR excess because it has a disk with strong H α emission. Recently, it was reported that young brown dwarfs have circumstellar disks, i.e., strong H α emission due to mass accretion (e.g., Luhman et al. 2007). If E1 actually has NIR excess, this extinction becomes an upper limit. This upper limit is similar to A_V of E2, which is located next to E1 and a little closer to BRC37.

We show the i' vs. $i' - J$ diagram with the isochrones of the NextGen model (Baraffe et al. 1998) in Fig. 10. Without any extinction correction, the location of E1 in this diagram indicates that it is a young brown dwarf. If we adopt the upper limit value, the mass and age are estimated to be $\sim 0.06 M_\odot$ and ~ 5.0 Myr, respectively. If E1 has extinction smaller than 2.0 mag., its mass and age become smaller. The derived age of ~ 5.0 Myr for E1 (assuming an upper limit for reddening) is somewhat larger than the estimated ages of E2, E3, E5, and E6 in Fig. 8.

With the Nextgen model, the ages and masses of E2, E3, E5, and E6 are estimated to be $\sim 2\text{--}8$ Myr and $\sim 0.8\text{--}1.2 M_\odot$, respectively. The values are somewhat larger than those from the model of Palla & Stahler (1999). Luhman et al. (2003) used the evolutionary model of Palla & Stahler (1999) for $M/M_\odot \geq 1$ and the NextGen model for $M/M_\odot \leq 1$. Following Luhman et al. (2003), we use the model of Palla & Stahler (1999) for E2, E3, E5, and E6 and we use the NextGen model for E1. From these comparisons, we conclude that E1 is most likely to be a young brown dwarf with an age of a few Myr.

For I6, no H α emission was detected. This suggests that I6 has no circumstellar disk, and therefore is not so young. If I6 is located at the distance of IC1396 (750pc), it would have a very small extinction (Fig. 9), and then would be plotted far above the isochrone of 1 Myr on Fig. 10. Specifically, if we assume a young age of ~ 10 Myr for I6, we can estimate its distance and mass to be ~ 240 pc and $\sim 0.03M_\odot$, respectively. Alternatively if I6 is very old ($\sim 1\text{--}10$ Gyr), a distance and mass of ~ 100 pc and $\sim 0.085M_\odot$ are indicated, i.e., a late M-dwarf. In either case we conclude that I6 is a foreground source.

In order to further examine E7–E10, we constructed the i' vs. $g' - i'$ and I_C vs. $V - I_C$ diagrams with the isochrones of Palla & Stahler (1999). E7, E8 and E10 are located below the isochrone of 10 Myr and therefore are likely to be background stars. From the $J - H$ and $H - K$ colors, E8 is likely to be a Herbig Ae/Be star or classical Be star. If extinction is large, E9 may be a background star. But if extinction is small, there is a possibility that E9 is a YSO associated with IC1396 with an age of $\sim 3\text{--}10$ Myr. We note that E9 shows variability: Its i' magnitude was measured at 17.7 on 2006 November 19 UT and its I_C magnitude was 16.1 on 2007 August 7 UT. We can expect an i-I difference for this red object

of ≤ 0.8 mag from the differences in photometric systems,² so the large measured difference (~ 1.6 mag.) indicates substantial brightening over this period.

In Table2, we summarize the YSO identifications in this work. Objects in the upper part of this table are the YSO candidates associated with the tip of BRC37 while those in the middle part are the YSO candidates located toward the tail part of BRC37. Objects in the lower part are considered to be background/foreground sources, except E9 whose uncertain status is discussed above.

4. Discussion

In this section, we discuss only the objects in the upper and middle parts of Table2 as YSO candidates of BRC37. In Fig. 11a, a closeup view toward the tip is shown with the labels of these YSOs including the IRAS source.

4.1. Sequential star formation in BRC37

The IRAS source is still driving the H₂ bow shocks and HH objects, and is considered to be a protostar-like object having a considerably young age, whereas the dynamical age of the molecular outflow was reported to be ~ 0.3 Myr (Duvert et al. 1990). On the other hand, the ages of E1–E3, E5, and E6, which are located at the globule tip facing the exciting star(s), are estimated to be ~ 1.0 Myr. These suggest that star formation has been taking place from the outside of the cloud toward the IRAS source.

In more detail, it seems that E6 and I1 are younger than the objects on the closer side of the exciting star(s), and are older than the IRAS source. They are located between E1–E3, and E5 and the IRAS source. While E1–E3, and E5 are outside the molecular cloud, E6 and I1 are embedded in the ¹³CO molecular gas (see Fig. 2 of Sugitani et al. 1997), and have considerably larger NIR excess than those outside sources. E6 has the [SII], [NII], and [OI] lines, while the other emission stars (E1–E3 and E5) do not show these lines, suggesting outflow activity and a younger age for E6. I1 has a NIR reflection nebula, which suggests association with a circumstellar envelope. However, since I1 and E6 do not show strong outflow activities like the IRAS source, they are older than the IRAS source. These findings indicate sequential star formation in order of E1–E3 then E5, E6 and I1, then the IRAS source from outside the cloud to the central source itself (Fig. 11b).

²Lupton (2005); <http://www.sdss.org/dr5/algorithms/sdssUBVRITransform.html#Lupton2005>

4.2. Direction of exciting sources

We examined the direction from the main exciting star to the IRAS source (UV incident angle) and the axis of the tip part of BRC37. We determined the axis/elongation direction by eye using the ^{13}CO maps of Sugitani et al. (1997). This elongation direction of ^{13}CO gas at its tip part (P.A. $\sim 165^\circ$) is nearly parallel to the direction of the UV radiation from the main exciting star to the IRAS source (P.A. = 166.6°). This suggests that the tip structure might have been strongly affected by the UV radiation as was discussed in Sugitani et al. (1997). The axis direction of the head part, which is a region of $\sim 1'.5$ long and includes the tip part, is estimated to have P.A. $\sim 147^\circ$ (Fig. 1) and slightly differs from the two directions above by $\sim 20^\circ$.

Interestingly, the YSOs are almost aligned along a straight line (Fig. 11a), whose direction (P.A. $\sim 147^\circ$) differs from that of the UV radiation from the main exciting star by $\sim 20^\circ$, but agrees with the axis direction of the head part (Table 3). Therefore, we searched for other exciting stars along the straight line from the YSOs toward the central region of IC1396, and found two candidates, which are members of Trumpler 37 (Garrison & Kormendy 1976), on a straight line of P.A. $\sim 143^\circ$. One is HD205794 (B0.5V) and another is HD206183 (O9.5V). The former is located toward the central region near the rim Ab cloud (Weikard et al. 1996) and the projected distance is $\sim 14\text{pc}$, while the latter is located at a closer position with a projected distance of $\sim 6\text{pc}$. Since the latter has an earlier type and is closer to BRC37, it is possibly another exciting star of BRC37. However, the flux of ionizing photons from the main O6 exciting star is estimated to be ~ 5 times larger than that from HD206183 (O9.5V) at the position of BRC37 and the impact from the main exciting star seems to be dominant at present. If the YSO alignment and the elongation of the head part were originally made under the influence of HD206183 (O9.5V), its impact might have been dominant *before* the main O6 exciting star became dominant. This suggests that the main O6 exciting star was born quite recently compared to HD206183 (O9.5V). The directions almost agree with each other with the small differences of $\lesssim 20^\circ$, and strongly indicates that these YSOs have been formed due to the strong UV impact of the main exciting star (O6) and/or HD206183 (O9.5V).

4.3. Timescale of star formation in BRC37

We can estimate the speed of propagation of the sequential star formation. The projected distance from E1 to the IRAS source is $\sim 0.2\text{ pc}$. Assuming a period of star formation of $\sim 10^6\text{yr}$, we derive a speed of propagation of $\sim 0.2\text{ km s}^{-1}$. This speed is comparable to that of the ionization front that would be created by HD206183 (O9.5V), if we assume a cloud

density of $n(\text{H}_2) \sim 10^3 \text{ cm s}^{-3}$. A shock would precede the ionization front with a somewhat larger speed to induce sequential star formation, if small cores preexisted at the cloud tip or were decoupled from the cloud tip due to the locally enhanced self-gravity introduced by its original density fluctuation (e.g., Kessel & Burkert 2003). On the other hand, the earlier type star HD206267 (O6) would create a significantly faster ionization front that could be too much to explain the speed of propagation of the sequential star formation. This again indicates that the YSO alignment is due to ionizing flux from HD206183 (O9.5V) and that HD206267 (O6) turned on quite recently.

The status of R1–R3 is less clear, but if we assume that R1–R3, located toward the ^{13}CO clumps in the tail of the BRC37 cloud, are really YSOs, this would imply that star formation might occur spontaneously in the tail of the BRC37 cloud without an external agitation. Since R1–R3 are Class I candidates, star formation in the tail might have begun quite recently compared to the tip region, suggesting that star formation lags in the tail. Since R1–R3 are faint, their masses may be much smaller than those of the tip sources. Such differences between the two regions could correspond to the difference between spontaneous and induced star formation, which lends support to the idea of induced star formation in the tip of the BRC37 cloud. Alternatively, if R1–R3 are background sources, then the lack of star formation in the tail would again support this idea.

4.4. A young brown dwarf candidate at the tip of BRC37

Since the obvious detections of brown dwarfs (Rebolo et al. 1995; Nakajima et al. 1995; Oppenheimer et al. 1995), many brown dwarfs have been found. However, it is still unclear how brown dwarfs form, e.g., whether dwarfs form in the same manner as stars or whether the formation mechanism differs from those of stars and planets. Two competing scenarios, ejection and turbulence scenarios, are well known as the formation mechanisms of brown dwarfs (e.g., Mohnsnty & Jayawardhana 2006). Recently, Whitworth et al. (2007) reviewed five mechanisms in detail, i.e., 1) turbulence fragmentation of molecular clouds, producing very low-mass prestellar cores by shock; 2) collapse and fragmentation of more massive prestellar cores; 3) circumstellar disk fragmentation; 4) premature ejection of protostellar embryos from their natal cores; and 5) photo-erosion of pre-existing cores overrun by HII regions. They mentioned that these mechanisms are not mutually exclusive and that their relative importance probably depends on environment. For the fifth mechanism, Whitworth et al. (2007) suggested that cores immersed in HII regions may be photo-eroded by the resulting ionization front and end up spawning brown dwarfs, from the calculations of Whitworth & Zinnecker (2004). Although Whitworth & Zinnecker (2004) noted that their

work was concerned with cores well within an HII region in the vicinity of the exciting star, the lower erosion rate may be expected even in cores of the periphery of the HII region.

As mentioned in Section 3.2, E1 is most likely to be a young brown dwarf with a circumstellar disk, which is located at the outer most position among the YSO candidates. Sequential star formation from the outside toward the inside is strongly suggested in this globule. Thus, E1 is very likely to have formed prior to the other candidates of T Tauri stars.

If so, it may be impossible for the brown dwarf to form with the mechanisms 3), because E1 is not a companion. Also, it may be impossible to form with the mechanism 4), because it could be very rare that the prestellar core of E1 was ejected just to the direction along the globule axis (direction of sequential star formation). If the prestellar core of E1 is formed by the mechanism 1) or 2) (e.g., Kessel & Burkert 2003), it should be inevitable that this core is exposed to the UV radiation and is photo-eroded. Therefore, we conclude that it is likely that mechanism 5) follows the mechanisms 1) and 2). If the photo-erosion rate was not high enough to form the brown dwarf from the prestellar core that forms a low-mass star, the initial mass of the prestellar core could be very small. And if the prestellar core was very small so that it was thermally supported, it could be squeezed by ionization shock front. Thus, the brown dwarf could be formed by the UV impact at the tip of BRC37.

However, it is difficult to definitely eliminate the possibility that it is a background $H\alpha$ source that is severely reddened. Spectroscopy of the outermost source is essential to confirm whether it is really a young brown dwarf.

5. Summary

We conducted near-IR (J , H , K_s , and H_2) and optical (g' , i' , wide $H\alpha$, V , I_C , and slitless grism spectroscopy) observations of BRC37. Our work is summarized as follows:

1. Ten $H\alpha$ emission stars (E1–E10) were detected around BRC37. Six of them (E1–E6) are located at the tip and aligned along the straight line that is parallel to the axis of the head part of BRC37. E2, E3, E5 and E6 are most likely to be CTTSs associated with the tip of BRC37.
2. NIR excess sources (I1–I6) were selected from the $J-H$ vs. $H-K$ color-color diagram. One (I1) of them seems to be a Class I source embedded in the tip of BRC37, while the other sources except I6 seem to be galaxies. It is possible that I6 is a foreground brown dwarf or late M-dwarf.

3. Three red NIR sources (R1–R3), which are detectable both at H and K_s , but not at J , are selected toward the ^{13}CO clumps as possible Class I candidates.
4. We detected H_2 emission that was probably excited by the outflows from the IRAS source, suggesting that the IRAS source is a protostar-like object having a considerably young age.
5. The ages of E2, E3, E5 and E6 are estimated to be ~ 1.0 Myr from the evolutionary model of pre-main sequence stars. This suggests that they were formed at the tip in advance of the formation of the IRAS source. The UV incident angles from the main exciting star (O6) of IC1396 and the closer exciting star (HD206183, O9.5) of BRC37, the axis angles of the head part and its tip of the BRC37 cloud, and the alignment angle of YSOs are nearly identical, indicating that the YSOs at the tip were formed under the influence of the UV radiation from the main exciting star and/or HD206183. Thus, it is likely that sequential star formation has been taking place from the side of the exciting star(s) toward the IRAS source due to the UV impact of the exciting star(s).
6. E1 is located at the closest position to the exciting star(s) and seems to be a young brown dwarf that was formed by the UV impact in advance of the formation of other YSOs at the tip.

We thank the staff at the UH 2.2-m telescope for supporting our observations. Use of the UH 2.2-m telescope for the WFGS2 observations is supported by NAOJ. This work was supported in part by Grant-in-Aid for Scientific Research (17039011, 19540242) from the Ministry of Education, Culture, Sports, Science and Technology.

REFERENCES

- Baba, D., Sato, S., Nagashima, C., Nishiyama, S., Kato, D., Haba, Y., Nagata, T., Nagayama, T., Tamura, M., & Sugitani, K. 2006, *AJ*, 132, 1692
- Baraffe, I., Chabrier, G., Allard, F., & Hauschild, P. H. 1998, *A&A*, 337, 403
- Bertodi, F. 1989, *ApJ*, 346, 735
- Bessell, M. S. 1979, *PASP*, 91, 589
- Bessell, M. S., & Brett, J. M. 1988, *PASP*, 100, 1134

- Bessell, M. S. 1991, *AJ*, 101, 662
- Carpenter, J. M. 2001, *AJ*, 121, 2851
- Cardelli, J. A., Clayton, G. C., Geoffrey, C., & Mathis, J. S. 1989, *ApJ*, 345, 245
- Cohen, J. G. et al. 1981, *ApJ*, 249, 481
- Duvert, G., Chernicharo, J., Bachiller, R., & Gomez-Gonzalez, J. 1990, *A&A*, 233, 190
- Elmegreen, B.G. 1998, in *Origins*, ASP Conf. Ser. 148, ed. C. E. Woodward, J. M. Shull, & H. A. Thronson, Jr. (San Francisco: ASP), 150
- Froebrich, D., Scholz, A., Eisloffel, J., & Murphy, G. C. 2005, *A&A*, 432, 575
- Garrison, R. F., & Kormendy, J., 1976 *PASP*, 865, 869
- Getman, K. V., Feigelson, E. D., Garmire, G., Broos, P., & Wang, J. 2007 *ApJ*, 654, 316
- Hodapp, K. W. et al. 1996, *New A*, 1, 177
- Jordi, K., Grebel, E. K., & Ammon, K. 2006, *A&A*, 460, 339
- Kessel-Deynet, O., & Burkert, A. 2003, *MNRAS*, 338, 545
- Landolt, A. U. 1992, *AJ*, 104, 340
- Lefloch, B., & Lazareff, B. 1994, *A&A*, 289, 559
- Luhman, K. L., Joergens, V., Lada, C., Muzerolle, J., Pascucci, I., White, R. 2007, in *Protostars & Planets V*, ed. B. Reipurth, D. Jewitt, & K. Keil (Tucson: Univ. Arizona Press), 443
- Luhman, K. L., Stauffer, J. R., Muench, A. A., Rieke, G., H., Lada, E., A., Bouvier, J., & Lada, C. J. 2003, *ApJ*, 593, 1093
- Lupton, R. 2005, Transformations between SDSS magnitudes and UBVRIc, available from <http://www.sdss.org/dr5/algorithms/sdssUBVRITransform.html#Lupton2005>
- Matthews, H. E. 1979, *A&A*, 75, 345
- Matuyanagi, I., Itoh, Y., Sugitani, K., Oasa, Y., Mukai, T., & Tamura, M. 2006, *PASJ*, 58, L29
- Meyer, M. R., Calvet, N., & Hillenbrand, L. A. 1997, *AJ*, 114, 288

- Miao, J., White, G. J., Nelson, R., Thompson, M., & Morgan, L. 2006, MNRAS, 369, 143
- Mohsnty, S. & Jayawardhana, R. 2006, Scientific American, 294, 38
- Morgan, L. K., Thompson, M. A., Urquhart, J. S., & White, G. J. 2008 \AA , 477, 557
- Motoyama, K., Umemoto, T., & Shang, H. 2007, A&A, 467, 657
- Nakajima, T. et al. 1995, Nature, 378, 463
- Nagashima, C. et al. 1999, in Star Formation 1999, ed. T. Nakamoto., (Nobeyama: Nobeyama Radio Observatory), 397
- Nagashima, C. et al. 2003, MNRAS, 343, 1263N
- Nagayama, T. et al. 2003, Proc. SPIE, 4841, 459
- Oppenheimer, B.R. et al. 1995, Science, 270, 1478
- Ogura, K., Sugitani, K., & Pickles, A. 2002, AJ, 123, 2597 (OSP)
- Persson, S. E., Murphy, D. C., Krzeminski, W., Roth, M., & Rieke, M. J. 1998, AJ, 116, 2475
- Palla, F. & Stahler, S. W. 1999, ApJ, 525, 772
- Rebolo, R., Zapatero Osorio M. R., & Martin, E. L. 1995, Nature, 377, 129
- Sandford, M. T., II, Whitaker, R. W., & Klein, R. I. 1982, ApJ, 260, 183
- Schwartz, R. D., Gyulbudaghian, A. L., & Wilking, B. A. 1991, AJ, 370, 263
- Smith, J. A. et al. 2003, AJ, 123, 2121
- Sugitani, K., Fukui, Y. & Ogura, K. 1991, ApJS, 77, 59
- Sugitani, K., Tamura, M., & Ogura, K. 1995, ApJ, 455, L39
- Sugitani, K., Morita, K., Nakano, M., & Ogura, K. 1997 AJ, 486, L141, L144
- Sugitani, K., Tamura, M., & Ogura, K. 1999, in Star Formation 1999, ed. T. Nakamoto., (Nobeyama: Nobeyama Radio Observatory), 358
- Uehara, M., et al. 2004, Proc. SPIE, 5492, 661

- Urquhart, J. S., Thompson, M. A., Morgan, L. K., Pestalozzi, M. R., White, G. J., & Muna, D. N. 2007 *Å*, 467, 1125
- Weikard, H., Wouterloot, J. G. A., Castets, A., Winnewisser, G., & Sugitani, K. 1996, *A&A*, 309, 581-611
- Whitworth, A., Bata, M.R., Nordlund, A., Reipurth, B., & Zinnecker, H. 2007, in *Protostars and Planets V*, ed. B. Reipurth, D. Jewitt, and K Keil (Tucson: University of Arizona Press), 459
- Whitworth, A. P. & Zinnecker, H. 2004, *A&A*, 427, 299
- Williams, R. J. R., Ward-Thompson, D., & Whitworth, A. P. 2001, *MNRAS*, 327, 788

Appendix

A. Correction for Table 5 of OSP

As was mentioned in Section 3.1.1, $H\alpha$ equivalent widths (EWs) of the $H\alpha$ emission stars presented in Table 5 of Ogura, Sugitani & Pickles (2002) were *not* scaled from pixels to angstroms, and the data presented there for BRC13 are a repetition of that for BRC12. Here we show a fully corrected version of Table 5 from OSP as an online table (Table 4). We recalculated EWs from the same slitless spectroscopic images as those in OSP with the methodology mentioned in the main text, and properly scaled. The coordinates of the $H\alpha$ emission stars were also redetermined with the USNO-B1.0 catalog. We attached remarks on spectroscopic status, e.g., contamination from near star(s), bright rim(s) or nebulosity, and continuum strength (weak, very weak, or invisible), which strongly relate to the reliability of EW. The stub version of Table 4 in the main text shows the data for BRC13.

In the course of this correction, we found some $H\alpha$ emission stars that have not been identified in OSP. We also listed these newly found stars by adding "N" to their object numbers.

Table 1. H α Emission Stars

Object	α (J2000.0)	δ (J2000.0)	EW [Å]	Remarks	EW (OSP 2002) ^a [Å]
E1	21 ^h 40 ^m 25 ^s .55	+56°36′38″.7	invisible cont.	OSP 37-1	invisible cont.
E2	21 ^h 40 ^m 25 ^s .97	+56°36′32″.1	14.9	OSP 37-2	18.4
E3	21 ^h 40 ^m 26 ^s .77	+56°36′23″.5	36.4	OSP 37-3	40.9
E4	21 ^h 40 ^m 27 ^s .43	+56°36′20″.0	... ^b		not visible
E5	21 ^h 40 ^m 28 ^s .69	+56°36′09″.4	87.4 ^c	OSP 37-7	78.8 ^c
E6	21 ^h 40 ^m 28 ^s .03	+56°36′05″.9	invisible cont.	OSP 37-6, [SII] λ 6731 [NII] λ 6584, [O] λ 6300	invisible cont.
E7	21 ^h 40 ^m 13 ^s .67	+56°40′49″.9	42.8		...
E8	21 ^h 40 ^m 32 ^s .33	+56°38′40″.4	13.9	OSP 37-8	14.4
E9	21 ^h 40 ^m 42 ^s .27	+56°31′13″.2	22.5		...
E10	21 ^h 40 ^m 43 ^s .52	+56°31′42″.6	invisible cont.		...

^aCalculated from the spectroscopic data of Ogura, Sugitani & Pickles (2002) in the same manner as this work.

^bNot estimated due to contamination from a neighboring star (OSP 37-5).

^cSmall contamination from a neighboring star and bright rim.

Table 2. Summary of YSO Identification

Candidates	g' [mag]	i' [mag]	V [mag]	I_C [mag]	J [mag]	H [mag]	K [mag]	A_V^a [mag]	Candidate Type	Location
E1	...	21.09±0.14	≥22.83	20.06±0.08	17.43±0.02	16.64±0.03	15.95±0.02	≤2.00 ^b	young brown dwarf	BRC37 tip
E2	17.40±0.04	15.04±0.06	16.77±0.02	14.39±0.03	12.68±0.02	11.76±0.02	11.30±0.02	2.21	CTTS	BRC37 tip
E3	18.87±0.05	16.09±0.07	18.50±0.03	15.56±0.03	13.34±0.02	12.25±0.02	11.58±0.02	3.02	CTTS	BRC37 tip
E5	18.57±0.05	16.11±0.07	17.93±0.02	15.33±0.03	13.59±0.02	12.66±0.02	12.17±0.02	2.25	CTTS	BRC37 tip
E6	22.03±0.15	18.94±0.05	≥22.06	18.02±0.06	15.09±0.02	13.58±0.02	12.45±0.02	5.36	CTTS	BRC37 tip
I1	20.99±0.03	19.07±0.01	17.24±0.01	...	Class I	BRC37 tip
R1	18.85±0.11 ^d	16.43±0.03 ^d	...	Class I ?	BRC37 tail ?
R2	18.45±0.09 ^d	17.31±0.06 ^d	...	Class I ?	BRC37 tail ?
R3	18.95±0.11 ^d	17.71±0.07 ^d	...	Class I ?	BRC37 tail ?
E4	21.17±0.13	17.30±0.09	15.28±0.02	14.02±0.02	13.34±0.02	5.10	variable star	background ^d
E7	20.53±0.06	18.47±0.05	20.02±0.03	17.95±0.03	background
E8	16.39±0.02	15.45±0.04	16.14±0.02	14.95±0.02	13.43±0.03 ^c	13.17±0.04 ^c	12.98±0.05 ^c	...	HAEBE/classical Be ?	background
E9	21.14±0.10	17.72±0.06	18.93±0.03	15.86±0.06	variable star	IC1396/background ?
E10	...	20.28±0.10	22.10±0.11	18.59±0.04	background
I2	...	20.50±0.11	≥22.23	19.78±0.12	16.27±0.05	14.70±0.05	13.70±0.04	...	galaxy	background
I3	...	19.91±0.08	21.90±0.11	19.22±0.04	16.79±0.02	15.89±0.02	15.29±0.02	...	galaxy	background
I4	...	≥21.49	≥22.61	≥20.76	17.72±0.05	16.60±0.05	15.76±0.05	...	galaxy ?	background
I5	...	≥22.66	≥22.23	≥21.94	18.49±0.06	17.38±0.05	16.45±0.06	...	galaxy	background
I6	...	19.64±0.07	≥22.69	18.62±0.03	15.95±0.02	15.37±0.02	14.85±0.02	...	brown dwarf/late M-dwarf ?	foreground

^aEstimated from $J - H$ vs. $H - K$ diagram (see §3.2).

^bEstimated from J vs. $J - H$ diagram (see §3.2).

^cFrom the 2MASS Point Source Catalog.

^dSIRIUS system.

Table 3. Directions of YSO Alignment, UV incidence, and Cloud Axes

Direction	P.A.	Size of Elongation	Projected Distance to BRC37	Ionizing Photon Flux ($\text{s}^{-1} \text{cm}^{-2}$)
YSO alignment	$\sim 147^\circ$	$\sim 1'$
UV incidence				
from HD206267 (O6)	166.6°	...	$\sim 12\text{pc}$	$\sim 3.7 \times 10^8$
from HD206183 (O9.5V)	142.7°	...	$\sim 6\text{pc}$	$\sim 6.5 \times 10^7$
Cloud axis				
Tip of head part (^{13}CO gas) ^a	$\sim 165^\circ$	$\sim 0.7'$
Head part (optical)	$\sim 147^\circ$	$\sim 1.5'$

^aSee Fig. 2 of Sugitani et al. (1997).

Table 4. Updated and Corrected Table 5 of Ogura, Sugitani, & Pickles (2002)

Object Number	α (J2000.0)	δ (J2000.0)	EW (Å)	Remarks
BRC 13				
1	03:00:43.77	60:40:04.5	20.4	
2	03:00:44.82	60:40:09.2	17.2	double star
3	03:00:45.33	60:40:39.5	14.5	
4	03:00:46.50	60:39:52.8	64.1	contam. fr. nr. stars
5	03:00:50.91	60:40:59.6	...	contam. fr. nr. star
6a	03:00:51.28	60:39:36.5	112.8	double star
6b	03:00:51.04	60:39:36.1	...	double star, weak cont.
7	03:00:51.67	60:39:49.0	23.4	contam. from brigh rim
8	03:00:52.21	60:40:34.2	58.6	weak cont., contam. from brigh rim
9	03:00:52.65	60:40:42.5	...	contam. fr. nr. star
10	03:00:52.71	60:39:31.9	24.1	contam. fr. bright rims
11	03:00:53.39	60:40:26.6	...	contam. fr. nr. stars
12	03:00:55.47	60:39:42.9	75.7	contam. fr. nr. stars
13	03:00:56.03	60:40:26.5	8.2	weak cont., contam. fr. nr. stars
14	03:01:02.18	60:39:34.5	72.7	weak cont.
15	03:01:07.40	60:40:40.0	44.8	weak cont., contam. from No. 16 star
16	03:01:07.59	60:40:41.5	159.4	weak cont., contam. from No. 15 star
17	03:01:08.10	60:39:01.9	36.6	very weak cont.
18	03:01:11.15	60:38:55.9	27.1	very weak cont.
19	03:01:11.51	60:40:56.8	61.5	very weak cont.
20	03:01:12.15	60:38:42.3	...	invisible cont.
21	03:01:22.76	60:39:40.5	16.0	
22N	03:00:54.48	60:39:39.2	11.7	

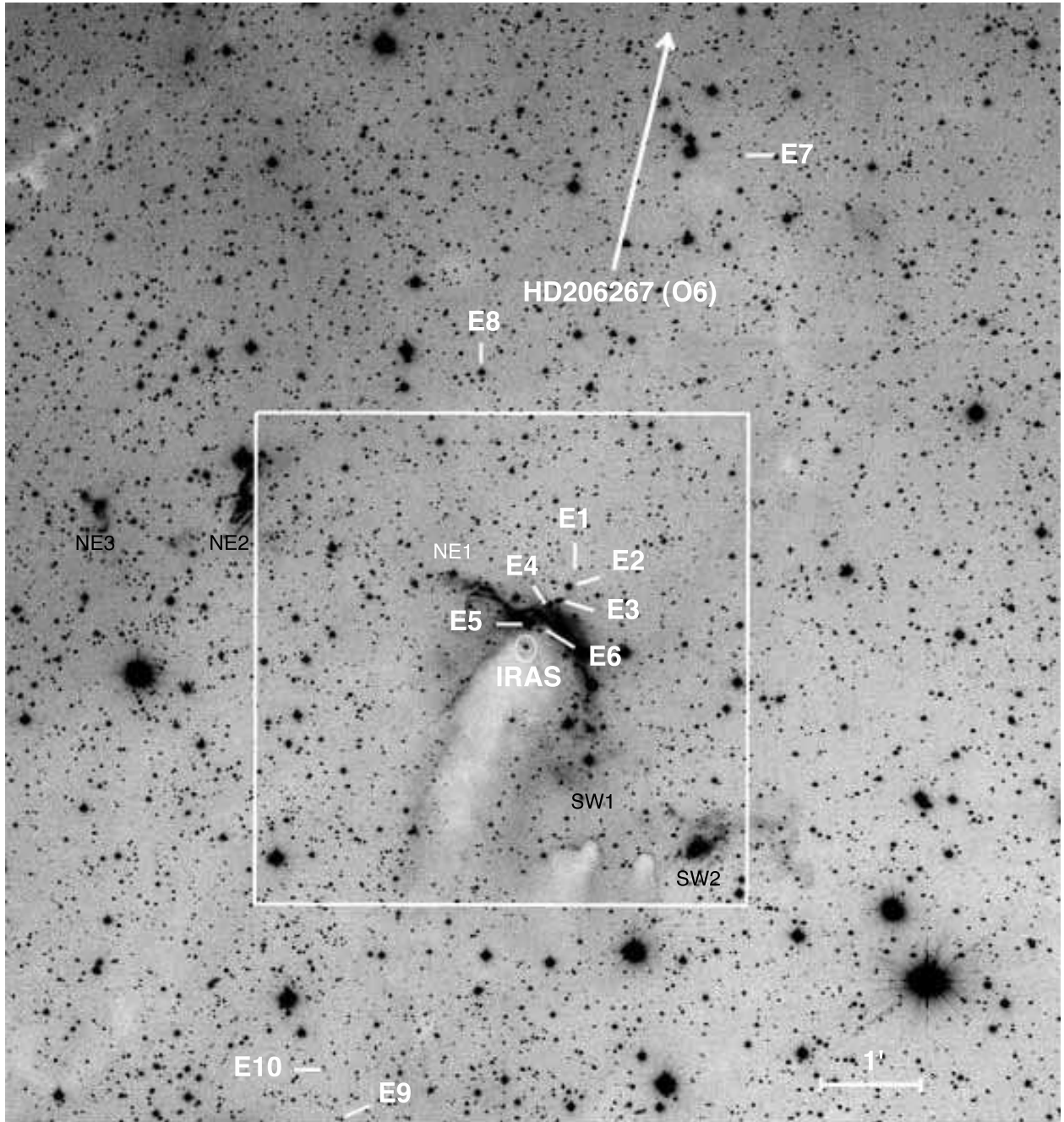


Fig. 1.— Image of BRC37 with wide $H\alpha$ filter. The position of IRAS 21388 + 5622 is shown with an error ellipse of position at the head part of the cometary globule. The size of the image is $11'.5 \times 11'.5$. The square is the region of the near-infrared observation. The $H\alpha$ emission stars are marked by E1-10. Known Herbig Haro objects are also indicated (HH588 NE1, NE2, SW1, and SW2 and NE3, Ogura, Sugitani & Pickles 2002; Froebrich et al. 2005, respectively). North is at the top and east to the left.



Fig. 2.— Three-color composite image of BRC37 (*J*, blue; *H*, green; *K_s*, red). The position of IRAS 21388 + 5622 is shown by an error ellipse of position. The size of the image is $\sim 4.7' \times 4.7'$. North is at the top, and east is to the left. Offsets in arc seconds from the position of $[\alpha(1950), \delta(1950)] = [21^{\text{h}}38^{\text{m}}54^{\text{s}}.02, +56^{\circ}21'33'']$, which is the same reference position of Duvert et al. (1990), are shown near the left and lower edges of the image. The blue color region at the upper right corner is dead pixel region of the *J* band array.

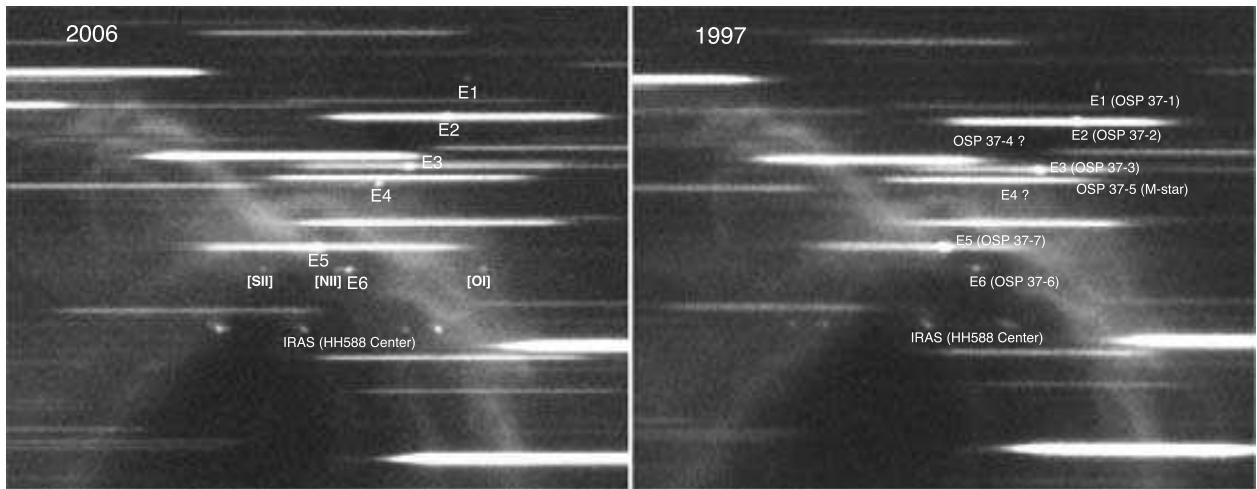


Fig. 3.— Slit-less spectroscopic images of the BRC37 tip of this work on 2006 November 19 UT (left) and Ogura, Sugitani & Pickles (2002) on 1997 August 10 UT (right). $H\alpha$ emission of each $H\alpha$ emission star is marked by the ID of this work (E1–E6) and the OSP IDs are also shown (right). The left image was obtained with WFGS2 + a wide $H\alpha$ filter (626.5–676.5 Å), and the right image with WFGS + a wide $H\alpha$ filter (6300–6750 Å). Although the dispersions of these images are the same ($3.8 \text{ \AA pixel}^{-1}$), the dispersion directions are different.

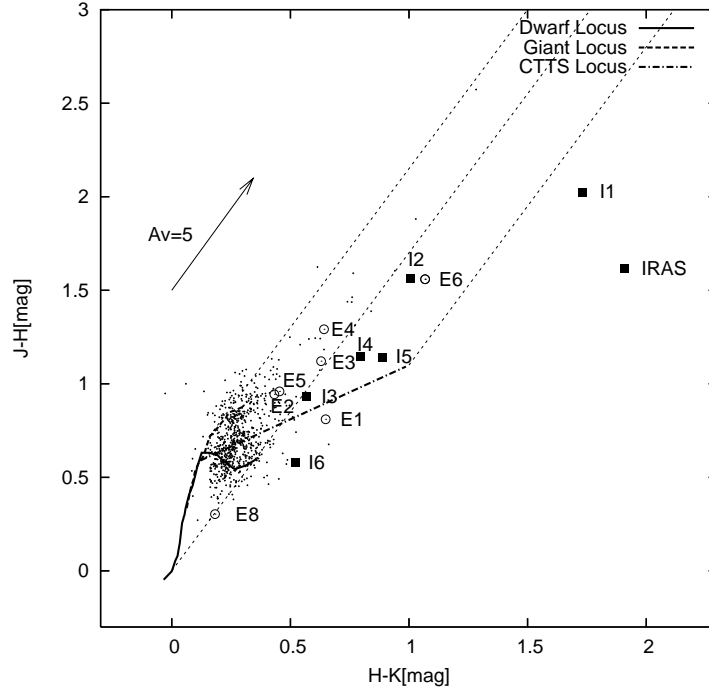


Fig. 4.— $J - H$ vs. $H - K$ color-color diagram of BRC37. The solid and dashed curves are the loci of dwarfs and giants, respectively. The data for O9–M6 dwarf and G0–M7 giants are from Bessel & Brett (1988). The dash-dotted line is the unreddened CTTS locus of Meyer et al. (1997). Only the sources having photometric errors in each color of ≤ 0.1 mag are plotted.

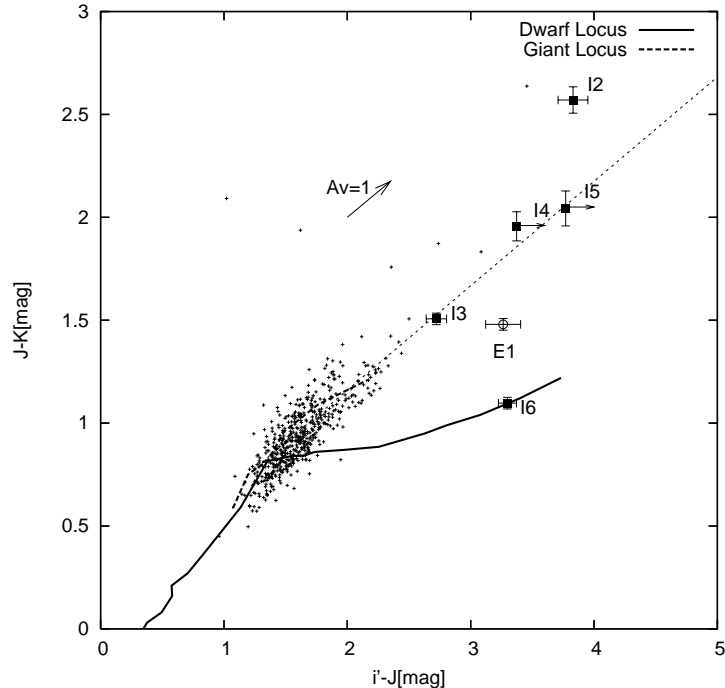


Fig. 5.— $J - K$ vs. $i' - J$ color-color diagram of BRC37. The solid and dashed curves are the loci of dwarfs and giants, respectively. The dwarf locus for B8–K2 and K7–M7 is from Bessel (1979, 1991). The giant locus for G6–M4.5 is from Bessel (1979). The thin dashed line is the unreddened CTTS locus from Meyer et al. (1997). Only the sources having photometric errors in each color of ≤ 0.1 mag are plotted.

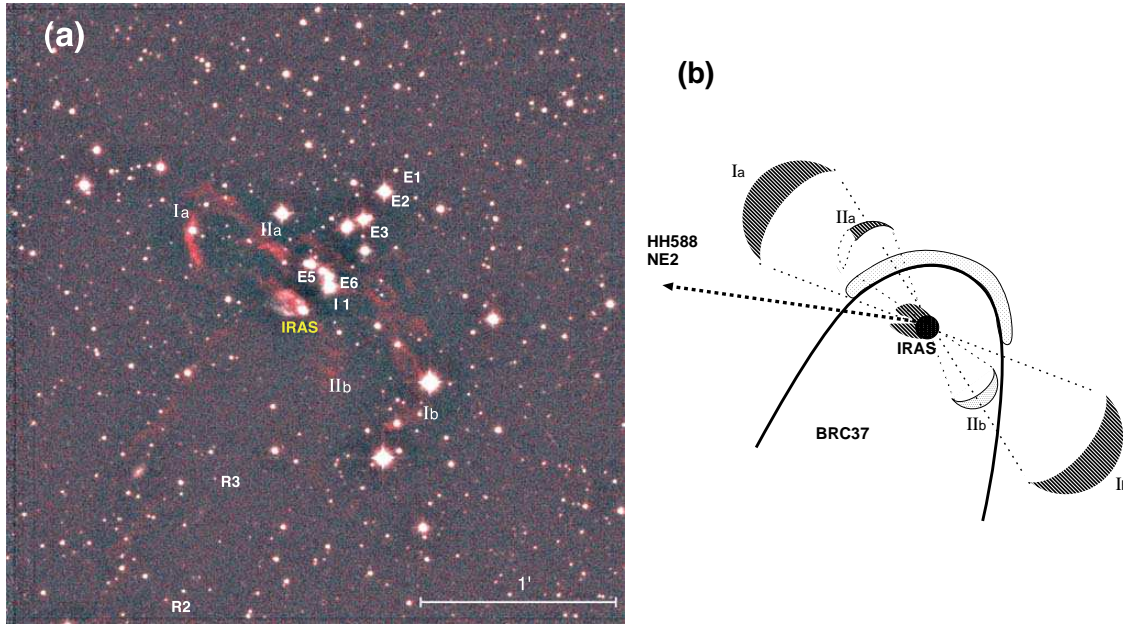


Fig. 6.— (a) False color image (cont., blue; cont., green; H₂+cont., red) of the BRC37. The size of image is $\sim 3.2' \times 3.2'$. (b) The schematic drawing of H₂ outflow structures.

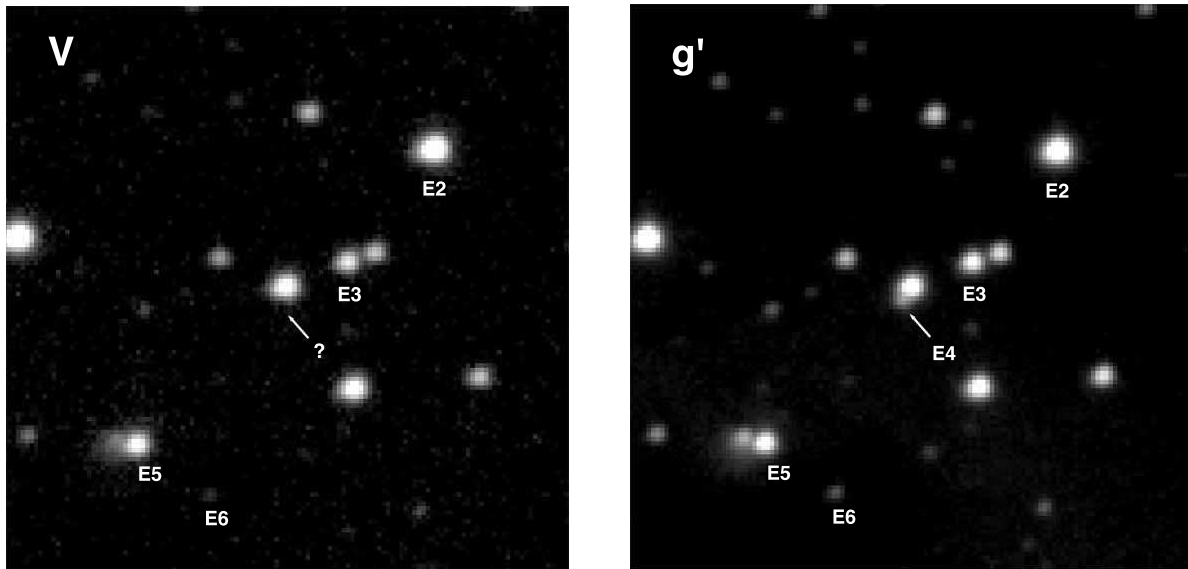


Fig. 7.— Images of E2–E6 at V (left) and g' (right) bands in logarithmic scale. E4 is clearly identified in the g' band image, but not in the V band image. The V band image was taken on 2007 August 7 UT and the g' band image on 2006 November 19 UT. North is at the top, and east is to the left. The size of each image is $\sim 42'' \times 42''$.

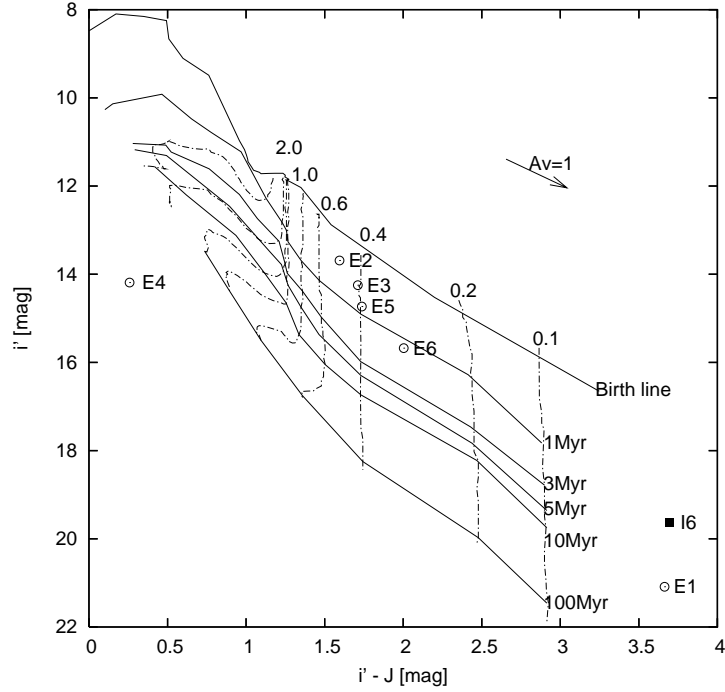


Fig. 8.— Extinction-corrected i' vs. $i' - J$ color-magnitude diagram of YSO candidates. $H\alpha$ emission stars are shown by open circles. The birthline and the 1, 3, 5, 10, and 100 Myr isochrones of Palla & Stahler (1999) are shown with the evolutionary tracks for masses from 0.1 to 2.0 M_{\odot} , at an assumed distance of 750pc. Extinction is not corrected for E1 and I6.

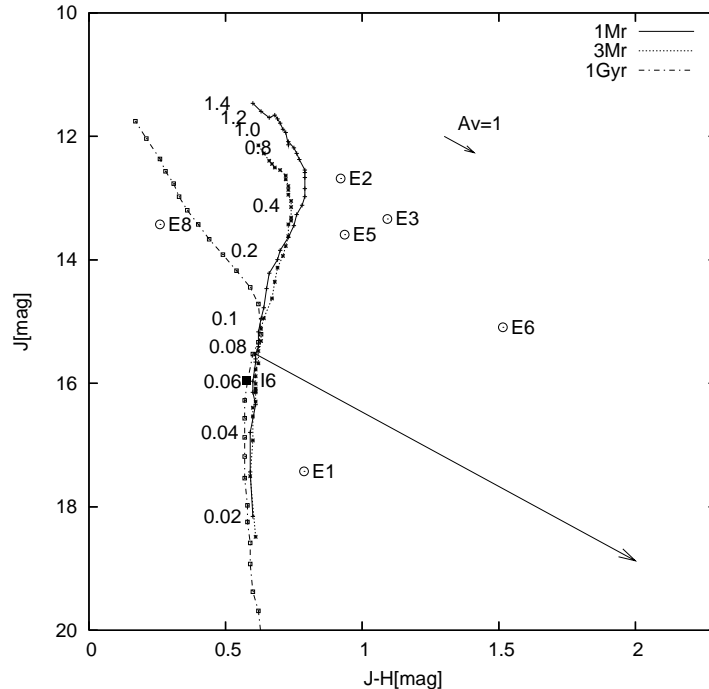


Fig. 9.— J vs. $J - H$ color-magnitude diagram of YSO candidates. $H\alpha$ emission stars are shown as open circles. The 1 Myr, 3 Myr and 1 Gyr isochrones of the NextGen model (Baraffe et al. 1998) at an assumed distance of 750pc are shown. The reddening line from a 0.075 M_{\odot} star of the 1 Myr locus is indicated (by arrow). The numbers near the 1 Myr

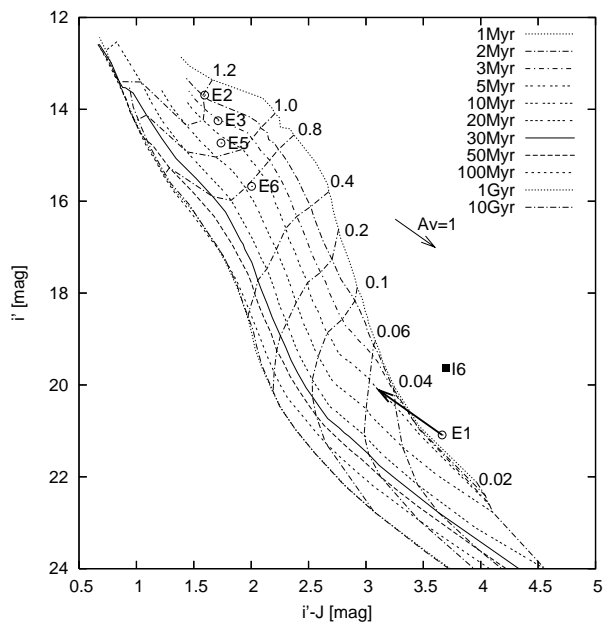


Fig. 10.— Extinction-corrected i' vs. $i' - J$ diagram of YSO candidates. The isochrones of the NextGen model (Baraffe et al. 1998) are shown with the evolutionary tracks for masses from 0.02 to 1.2 M_{\odot} at an assumed distance of 750pc.

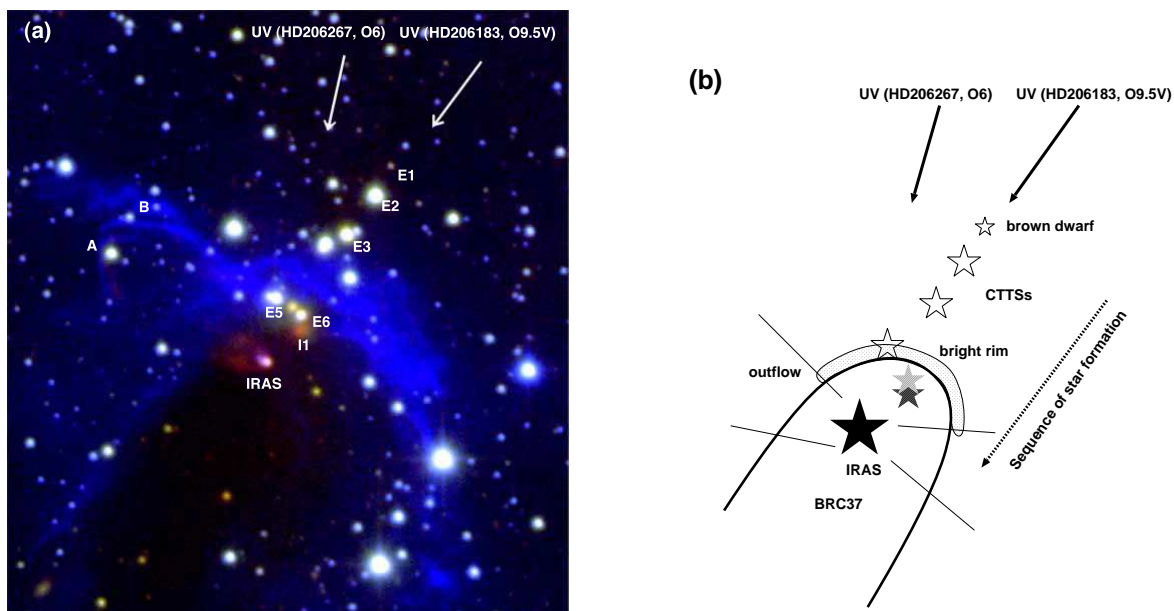


Fig. 11.— (a) Three composite image (wide $H\alpha$, blue; H , green; K_s , red) of the closeup of the tip of BRC37 and (b) the schematic drawing. The knots A and B of HH588 NE1 are marked by labels A and B. The size of image is $\sim 2.0' \times 2.0'$.

Online Material

Table 4. Updated and Corrected Table 5 of Ogura, Sugitani, & Pickles (2002)

Object Number	α (J2000.0)	δ (J2000.0)	EW (\AA)	Remarks
BRC 1				
1	23:59:42.50	67:22:27.8	...	invisible cont., contam. fr. nr. star
2	23:59:43.72	67:25:50.0	26.6	weak cont.
3	23:59:43.99	67:22:46.8	...	invisible cont.
4	23:59:47.61	67:23:11.2	...	H α ?, invisible cont.
5	23:59:47.98	67:23:06.9	...	H α ?, weak cont.
6	23:59:52.75	67:25:37.5	32.6	weak cont.
BRC 2				
1	00:03:51.03	68:33:15.8	...	H α ?
2	00:03:52.32	68:31:58.8	...	invisible cont.
3	00:03:54.52	68:33:44.6	...	contam. fr. nr. strs
4	00:03:54.98	68:32:42.8	145.7	very weak cont.
5	00:03:57.12	68:33:46.7	15.6	
6	00:03:57.35	68:33:23.0	99.6	
7	00:03:58.33	68:34:06.5	13.1	
8	00:03:59.12	68:32:47.3	18.2	
9	00:04:01.70	68:34:13.8	2.8	
10	00:04:01.81	68:34:00.0	14.0	
11	00:04:01.80	68:34:37.4	5.5	
12	00:04:01.88	68:34:34.5	21.2	
13	00:04:02.32	68:31:36.2	...	H α ?
14	00:04:02.65	68:34:26.6	24.9	
15	00:04:04.69	68:33:49.3	25.8	weak cont.
16	00:04:04.59	68:34:52.2	23.0	
17	00:04:05.28	68:33:56.0	136.6	very weak cont.
18	00:04:05.26	68:33:53.1	50.4	
19	00:04:05.66	68:33:44.3	94.5	

Table 4—Continued

Object Number	α (J2000.0)	δ (J2000.0)	EW (\AA)	Remarks
20	00:04:07.33	68:33:42.3	...	invisible cont.
21	00:04:07.60	68:33:25.1	12.8	
22	00:04:11.66	68:33:25.4	46.7	
23	00:04:13.97	68:32:21.8	85.7	weak cont.
24	00:04:14.71	68:32:49.1	42.1	
25	00:04:15.18	68:33:02.0	16.1	
26	00:04:15.41	68:34:05.5	26.6	very weak cont.
27	00:04:21.66	68:30:59.6	...	H α ?
28	00:04:25.36	68:32:31.0	12.3	weak cont.
29	00:04:29.99	68:31:19.9	...	H α ?
30N	00:03:59.88	68:33:41.7	1.4	
BRC 5				
1	02:28:44.20	61:31:15.4	6.0	
2	02:28:48.30	61:32:31.0	...	invisible cont.
3	02:28:53.81	61:33:32.3	39.2	weak cont.
4	02:28:59.11	61:32:48.8	85.5	
5	02:29:00.18	61:31:57.5	...	weak cont.
6	02:29:01.51	61:33:29.2	61.6	
7	02:29:05.68	61:32:59.2	...	contam. fr. nr. star
8	02:29:05.31	61:33:22.4	...	invisible cont.
9	02:29:08.13	61:34:09.9	198.0	very weak cont.
10	02:29:08.30	61:33:26.2	58.2	very weak cont.
11	02:29:14.16	61:33:25.8	86.5	
12N	02:28:46.50	61:35:59.8	...	contam. fr. No. 13 star
13N	02:28:45.52	61:36:01.0	39.1	contam. fr. No. 12 star
BRC 7				

Table 4—Continued

Object Number	α (J2000.0)	δ (J2000.0)	EW (\AA)	Remarks
1	02:34:28.32	61:47:43.5	...	contam. fr. nr. star
2	02:34:36.26	61:45:43.1	...	M-star ?
3	02:34:41.37	61:46:34.0	...	contam. fr. nr. star
4	02:34:58.17	61:46:48.6	...	very weak cont.
5	02:35:00.36	61:46:19.1	1.9	
6	02:35:03.50	61:49:01.9	9.9	
7	02:35:15.30	61:48:03.3	85.2	
8	02:35:15.31	61:48:09.5	16.5	
9	02:35:16.01	61:47:02.4	...	invisible cont.
10N	02:34:42.47	61:49:41.7	105.0	weak cont.
11N	02:34:41.67	61:50:00.7	29.1	
12N	02:34:34.35	61:47:47.0	...	invisible cont.
13N	02:34:29.28	61:47:47.2	...	invisible cont.
14N	02:34:32.81	61:46:36.9	53.0	very weak cont., contam. fr. nr. stars
BRC 11				
1	02:51:32.85	60:03:54.0	6.7	
BRC 11NE				
1	02:51:37.39	60:06:26.8	26.1	
2	02:51:47.33	60:07:47.2	6.3	
3	02:51:54.21	60:07:46.2	...	invisible cont.
4	02:51:54.52	60:08:26.8	76.5	contam. fr. nr. star
5	02:51:58.70	60:08:06.0	6.6	
6	02:51:59.77	60:06:39.4	12.1	weak cont.
7	02:52:11.12	60:07:15.3	15.7	
8	02:52:15.03	60:05:18.8	...	contam. fr. nr. stars
9N	02:51:55.02	60:07:17.4	109.0	

Table 4—Continued

Object Number	α (J2000.0)	δ (J2000.0)	EW (\AA)	Remarks
10N	02:51:52.16	60:07:10.2	44.6	
11N	02:51:51.64	60:07:30.6	...	contam. fr. nr. stars
12N	02:51:51.70	60:06:43.7	5.2	
BRC 11E				
1	02:52:13.64	60:03:26.2	245.1	very weak cont.
2	02:52:15.01	60:05:19.4	...	contam. fr. nr. stars
3N	02:52:14.25	60:03:11.7	55.4	
BRC 12				
1	02:54:45.06	60:35:38.3	5.1	
2	02:54:45.45	60:34:19.4	46.5	
3	02:54:46.21	60:34:40.9	...	invisible cont.
4	02:54:46.29	60:36:14.8	...	invisible cont., contam. fr. nr. star
5	02:54:49.51	60:38:26.1	4.5	weak $H\alpha$?
6	02:54:50.15	60:37:30.6	...	invisible cont.
7	02:54:50.51	60:37:28.7	...	$H\alpha$?, weak cont.
8	02:54:54.53	60:35:00.1	...	invisible cont.
9	02:54:56.52	60:35:45.8	18.6	contam. fr. nr. star
10	02:54:56.85	60:38:14.1	...	very weak cont.
11	02:54:58.05	60:35:51.0	57.0	contam. fr. bright rim
12	02:54:59.97	60:35:09.6	...	weak $H\alpha$?, contam. fr. bright rim
13	02:55:04.51	60:37:27.4	...	invisible cont.
14	02:55:07.80	60:36:19.9	33.2	contam. fr. nr. star
15	02:55:07.92	60:36:17.9	...	invisible cont.
16	02:55:09.67	60:36:21.0	...	contam. fr. nr. star
17	02:55:14.36	60:36:50.0	...	contam. fr. nr. star
18	02:55:16.04	60:35:15.5	...	very weak cont.

Table 4—Continued

Object Number	α (J2000.0)	δ (J2000.0)	EW (Å)	Remarks
19	02:55:16.98	60:38:02.3	57.2	contam. fr. nr. star
20	02:55:18.61	60:35:21.9	51.7	
21	02:55:18.75	60:36:09.4	86.2	contam. fr. nr. stars
22	02:55:19.10	60:36:09.5	...	contam. fr. nr. stars
23	02:55:20.23	60:35:14.3	...	invisible cont.
24	02:55:20.74	60:38:17.7	100.9	weak cont.
25N	02:54:58.72	60:35:48.4	75.5	contam. fr. bright rim
<hr/>				
BRC 13				
<hr/>				
1	03:00:43.77	60:40:04.5	20.4	
2	03:00:44.82	60:40:09.2	17.2	double star
3	03:00:45.33	60:40:39.5	14.5	
4	03:00:46.50	60:39:52.8	64.1	comtam. fr. nr. stars
5	03:00:50.91	60:40:59.6	...	contam. fr. nr. star
6a	03:00:51.28	60:39:36.5	112.8	double star
6b	03:00:51.04	60:39:36.1	...	double star, weak cont.
7	03:00:51.67	60:39:49.0	23.4	contam. from brigh rim
8	03:00:52.21	60:40:34.2	58.6	weak cont., contam. from brigh rim
9	03:00:52.65	60:40:42.5	...	contam. fr. nr. star
10	03:00:52.71	60:39:31.9	24.1	contam. fr. bright rims
11	03:00:53.39	60:40:26.6	...	comtam. fr. nr. stars
12	03:00:55.47	60:39:42.9	75.7	comtam. fr. nr. stars
13	03:00:56.03	60:40:26.5	8.2	weak cont., comtam. fr. nr. stars
14	03:01:02.18	60:39:34.5	72.7	weak cont.
15	03:01:07.40	60:40:40.0	44.8	weak cont., comtam. from No. 16 star
16	03:01:07.59	60:40:41.5	159.4	weak cont., comtam. from No. 15 star
17	03:01:08.10	60:39:01.9	36.6	very weak cont.
18	03:01:11.15	60:38:55.9	27.1	very weak cont.
19	03:01:11.51	60:40:56.8	61.5	very weak cont.

Table 4—Continued

Object Number	α (J2000.0)	δ (J2000.0)	EW (\AA)	Remarks
20	03:01:12.15	60:38:42.3	...	invisible cont.
21	03:01:22.76	60:39:40.5	16.0	
22N	03:00:54.48	60:39:39.2	11.7	
BRC 14				
1	03:01:04.06	60:31:26.1	44.2	weak cont.
2	03:01:05.84	60:28:03.1	47.5	very weak cont.
3	03:01:06.17	60:30:17.9	83.0	weak cont.
4	03:01:06.56	60:30:36.3	...	invisible cont.
5	03:01:07.74	60:29:21.9	38.0	
6	03:01:11.49	60:30:46.5	108.6	very weak cont.
7	03:01:13.00	60:28:51.7	102.1	contam. fr. nr. star
8	03:01:13.39	60:29:32.1	19.8	weak cont.
9	03:01:13.42	60:29:44.2	...	invisible cont.
10	03:01:16.12	60:29:47.1	...	contam. fr. nr. star
11	03:01:16.34	60:28:40.0	87.0	very weak cont.
12	03:01:17.06	60:29:23.2	13.5	
13	03:01:17.16	60:30:46.2	...	invisible cont.
14	03:01:17.73	60:29:32.0	...	contam. fr. nr. star
15	03:01:18.58	60:29:54.6	...	invisible cont.
16	03:01:18.76	60:29:56.4	...	H α ?, contam. fr. nr. star
17	03:01:19.91	60:30:11.6	38.3	weak cont., contam. fr. nr. star
18	03:01:20.26	60:30:02.2	...	contam. fr. nr. stars
19	03:01:20.67	60:29:54.6	...	contam. fr. nr. star
20	03:01:20.61	60:29:31.8	...	contam. fr. nr. stars
21	03:01:20.58	60:29:28.0	...	invisible cont.
22	03:01:20.86	60:29:46.5	...	contam. fr. nr. stars
23	03:01:21.16	60:29:44.3	107.0	contam. fr. nr. star
24	03:01:21.22	60:30:10.4	...	contam. fr. nr. star

Table 4—Continued

Object Number	α (J2000.0)	δ (J2000.0)	EW (\AA)	Remarks
25	03:01:21.59	60:28:56.6	22.1	
26	03:01:22.38	60:30:02.9	...	contam. fr. nr. star and bright rim
27	03:01:23.48	60:30:50.4	...	invisible cont.
28	03:01:23.82	60:29:58.5	...	contam. fr. bright rim
29	03:01:24.01	60:30:42.5	...	contam. fr. nr. star
30	03:01:24.73	60:30:09.6	...	weak cont., contam. fr. bright rim
31	03:01:25.57	60:29:39.0	14.0	
32	03:01:26.39	60:30:53.9	10.1	
33	03:01:27.20	60:30:56.8	29.8	weak cont.
34	03:01:27.41	60:30:39.4	...	contam. fr. nr. star and bright rim
35	03:01:29.29	60:31:13.6	55.9	
36	03:01:30.43	60:31:02.5	99.1	very weak cont.
37	03:01:31.00	60:30:26.9	...	invisible cont., contam. fr. nr. stars
38	03:01:31.19	60:30:20.8	...	weak H α ?, contam. fr. nr. star
39	03:01:33.92	60:27:45.9	9.8	
40	03:01:34.33	60:30:08.5	14.5	
41	03:01:36.36	60:29:06.1	30.9	contam. fr. nr. star
42	03:01:36.91	60:31:00.1	22.6	contam. fr. No. 44 star
43	03:01:37.03	60:29:41.1	5.3	M-star ?
44	03:01:36.96	60:31:01.2	...	contam. fr. No. 42 star
45	03:01:37.54	60:28:54.0	...	invisible cont.
46	03:01:43.27	60:28:51.3	...	H α ?
47	03:01:49.88	60:28:50.7	31.3	weak cont.
48N	03:01:20.31	60:29:49.2	6.2	
49N	03:01:23.51	60:31:51.0	...	invisible cont., near upper edge
50N	03:01:05.22	60:31:55.5	59.2	cor. fr. DSS II R

BRC 27

1	07:03:52.49	-11:26:16.9	17.5
---	-------------	-------------	------

Table 4—Continued

Object Number	α (J2000.0)	δ (J2000.0)	EW (\AA)	Remarks
2	07:03:52.70	-11:23:13.5	...	double star
3	07:03:53.22	-11:24:03.8	...	invisible cont.
4	07:03:53.72	-11:24:28.7	30.2	
5	07:03:54.98	-11:25:14.6	13.3	
6	07:03:56.37	-11:25:41.4	...	H α ?, double star, contam. fr. nr. star
7	07:03:57.11	-11:24:32.9	...	H α ?
8	07:04:02.86	-11:23:37.4	15.6	contam. fr. No. 9 star
9	07:04:02.93	-11:23:39.1	8.1	contam. fr. No. 8 star
10	07:04:03.07	-11:23:50.8	36.4	contam. fr. nr. star and bright rim
11	07:04:04.07	-11:26:35.4	23.2	weak cont.
12	07:04:04.24	-11:23:55.9	166.5	weak cont.
13	07:04:04.57	-11:25:55.0	3.8	H α ?
14	07:04:04.68	-11:23:40.0	10.4	
15	07:04:05.19	-11:23:13.5	33.2	contam. fr. nr. stars
16	07:04:05.91	-11:23:58.9	25.0	bad pix. at H α
17	07:04:06.02	-11:23:16.0	...	contam. fr. No. 19 star
18	07:04:06.43	-11:23:36.3	109.0	weak cont., contam. fr. nr. star
19	07:04:06.55	-11:23:16.6	14.0	contam. fr. nr. stars (incl. No. 17 star) and bright rim
20	07:04:06.68	-11:26:08.5	54.1	
21	07:04:07.96	-11:23:11.8	...	H α ?, contam. fr. nr. stars
22	07:04:08.02	-11:23:54.9	38.9	
23	07:04:08.16	-11:23:09.8	231.2	weak cont.
24	07:04:09.24	-11:24:38.3	44.0	weak cont.
25	07:04:09.94	-11:23:16.6	53.4	
26	07:04:10.93	-11:23:27.6	...	H α ?, contam. fr. nr. star
27	07:04:11.95	-11:24:22.9	62.1	weak cont.
28	07:04:12.75	-11:24:03.5	182.2	weak cont., contam. fr. nr. star
29	07:04:13.52	-11:24:55.9	16.9	
30	07:04:13.91	-11:24:41.8	12.9	
31	07:04:14.25	-11:23:17.1	30.2	near image edge

Table 4—Continued

Object Number	α (J2000.0)	δ (J2000.0)	EW (Å)	Remarks
32	07:04:14.27	-11:23:37.3	...	weak cont., near image edge
33N	07:04:02.23	-11:25:43.0	8.8	
BRC 30				
1	18:18:35.35	-13:45:48.0	15.2	
2	18:18:35.51	-13:48:25.9	92.2	weak cont.
3	18:18:36.33	-13:49:06.3	...	very weak cont.
4	18:18:36.52	-13:49:30.1	6.6	M-star ?
5	18:18:37.26	-13:48:26.2	24.7	M-star ?, weak cont.
6	18:18:37.27	-13:50:13.7	65.5	weak cont.
7	18:18:37.30	-13:45:57.0	...	contam. fr. nr. star
8	18:18:37.65	-13:46:06.4	...	contam. fr. nr. star
9	18:18:37.69	-13:46:08.4	...	contam. fr. nr. star
10	18:18:38.25	-13:47:40.3	...	invisible cont.
11	18:18:38.24	-13:51:17.1	62.3	
12	18:18:38.35	-13:47:33.4	...	contam. fr. nr. star
13	18:18:38.60	-13:49:24.3	...	invisible cont.
14	18:18:38.72	-13:47:10.3	...	contam. fr. nr. stars
15	18:18:38.81	-13:46:44.3	...	saturated
16	18:18:39.33	-13:46:54.4	...	contam. fr. nr. stars
17	18:18:39.41	-13:48:08.2	...	invisible cont.
18	18:18:39.74	-13:47:48.1	...	weak cont., contam. fr. nr. stars
19	18:18:40.08	-13:47:00.8	5.0	
20	18:18:40.11	-13:46:31.3	13.3	contam. fr. nr. star
21	18:18:41.25	-13:49:14.2	...	very weak cont., contam. fr. nr. stars
22	18:18:41.34	-13:45:44.8	8.6	
23	18:18:41.40	-13:48:35.8	...	invisible cont.
24	18:18:41.51	-13:48:10.9	136.3	very weak cont.
25	18:18:41.48	-13:45:53.7	...	H α ?

Table 4—Continued

Object Number	α (J2000.0)	δ (J2000.0)	EW (\AA)	Remarks
26	18:18:41.63	-13:50:13.2	89.9	
27	18:18:41.66	-13:47:12.6	...	contam. fr. nr. star
28	18:18:41.87	-13:47:21.4	...	contam. fr. nr. stars (incl. No. 31 star)
29	18:18:41.93	-13:48:59.8	3.4	
30	18:18:42.02	-13:49:42.3	85.1	
31	18:18:42.17	-13:47:22.4	...	contam. fr. nr. stars (inc. No. 28 star)
32	18:18:42.33	-13:49:54.2	27.4	weak cont.
33	18:18:42.41	-13:46:10.9	...	weak cont., contam. fr. nebula
34	18:18:42.53	-13:47:15.5	...	contam. fr. nr. stars (incl. No. 36)
35	18:18:42.82	-13:47:27.9	22.2	contam. fr. nr. star
36	18:18:43.02	-13:47:15.2	...	[NII], contam. fr. nr. stars (incl. No. 34)
37	18:18:43.02	-13:49:50.6	27.2	
38	18:18:43.19	-13:46:39.2	19.4	
39	18:18:43.28	-13:50:03.4	63.3	
40	18:18:43.80	-13:46:09.5	40.0	contam. fr. nr. star
41	18:18:43.82	-13:48:04.3	...	invisible cont., contam. fr. nr. star
42	18:18:44.01	-13:46:38.0	...	weak cont., contam. fr. nr. stars
43	18:18:44.20	-13:48:17.6	7.1	
44	18:18:44.44	-13:50:58.5	...	weak cont., contam. fr. nebulosity
45	18:18:44.63	-13:48:00.5	...	weak cont., contam. fr. nr. star
46	18:18:44.84	-13:47:48.5	...	contam. fr. nr. star
47	18:18:44.88	-13:49:03.7	...	double star, contam. fr. nebulosity
48	18:18:45.04	-13:47:52.2	...	contam. fr. nr. star
49	18:18:45.18	-13:48:37.4	14.1	
50	18:18:45.30	-13:48:40.1	...	H α ?
51	18:18:45.65	-13:46:56.9	7.8	contam. fr. nr. star
52	18:18:45.86	-13:46:53.8	6.3	contam. fr. nr. star
53	18:18:46.02	-13:47:30.2	43.1	contam. fr. nebulosity
54	18:18:46.05	-13:47:10.9	...	H α ?, contam. fr. nr. star
55	18:18:46.29	-13:48:09.1	...	invisible cont.

Table 4—Continued

Object Number	α (J2000.0)	δ (J2000.0)	EW (\AA)	Remarks
56	18:18:46.31	-13:49:26.7	...	very weak cont., contam. fr. nr. star
57	18:18:46.80	-13:49:32.0	8.5	
58	18:18:46.86	-13:49:16.5	7.8	
59	18:18:47.02	-13:49:29.2	16.4	
60	18:18:47.96	-13:48:36.3	112.4	contam. fr. nr. stars
61	18:18:48.10	-13:48:20.2	11.4	weak cont., contam. fr. nebulosity
62	18:18:48.20	-13:49:08.3	31.5	
63	18:18:48.39	-13:45:49.8	...	H α ?
64	18:18:48.64	-13:47:49.7	17.3	contam. fr. nebulosity
65	18:18:48.91	-13:48:32.3	20.2	weak cont., contam. fr. nebulosity
66	18:18:49.76	-13:47:46.5	...	H α ?
67	18:18:49.88	-13:46:59.7	7.8	
68	18:18:52.10	-13:48:10.3	14.0	contam. fr. nr. star
69	18:18:52.24	-13:46:39.1	20.2	
70	18:18:52.39	-13:46:58.5	6.6	
71	18:18:52.81	-13:48:36.9	85.0	weak cont.
72	18:18:53.05	-13:46:18.6	39.7	
73	18:18:54.52	-13:47:17.3	8.7	
74	18:18:55.04	-13:46:44.6	25.4	
75	18:18:55.30	-13:46:51.8	...	contam. fr. nr. star
76	18:18:57.75	-13:44:42.4	...	contam. fr. nr. star
77	18:18:58.52	-13:42:45.9	21.1	contam. fr. nr. star
78	18:18:58.50	-13:48:28.6	8.0	
79	18:18:59.18	-13:45:58.5	...	invisible cont.
80	18:19:01.08	-13:45:20.9	38.9	very weak cont.
81	18:19:01.46	-13:44:42.6	...	invisible cont.
82	18:19:01.60	-13:45:16.3	4.5	

Table 4—Continued

Object Number	α (J2000.0)	δ (J2000.0)	EW (\AA)	Remarks
1	20:50:36.94	44:21:41.0	49.9	
2	20:50:36.98	44:20:50.1	29.3	
3	20:50:37.37	44:20:53.3	7.5	
4	20:50:37.47	44:21:16.2	60.0	
5	20:50:40.45	44:20:22.1	66.3	
6	20:50:40.54	44:20:51.0	27.3	contam. fr. bright rim
7	20:50:42.72	44:21:53.4	39.1	weak cont., contam. fr. No. 8 star
8	20:50:42.81	44:21:55.5	...	double star, both show H α emission
9	20:50:44.97	44:20:59.4	28.9	weak cont.
10	20:50:45.40	44:21:49.9	32.7	very weak cont., contam. fr. bright rim
11	20:50:48.59	44:21:05.0	14.4	
12	20:50:48.63	44:20:25.4	...	H α ?
13	20:50:48.70	44:20:53.7	27.2	
14	20:50:50.40	44:21:39.0	...	H α ?
15	20:50:50.96	44:23:46.8	75.4	weak cont., contam. fr. bright rim
16	20:50:51.26	44:21:32.0	31.4	weak cont.
17	20:50:51.72	44:20:46.4	...	invisible cont.
18	20:50:53.17	44:23:53.8	14.1	
19	20:50:53.60	44:22:12.7	...	star ?, H α ?
20	20:50:53.53	44:24:27.2	12.5	
21	20:50:53.58	44:21:01.4	9.0	
22	20:50:53.62	44:24:30.9	22.1	
23	20:50:53.85	44:21:40.3	...	contam. fr. nr. stars
24	20:50:53.73	44:21:18.9	...	contam. fr. No. 25 star
25	20:50:53.94	44:21:18.9	...	contam. fr. No. 24 star
26	20:50:54.89	44:22:58.5	91.8	
27	20:50:54.86	44:20:13.1	31.5	
28	20:50:55.58	44:24:24.9	121.6	very weak cont., contam. fr. No. 20 star
29	20:50:58.74	44:23:17.7	99.0	
30	20:51:02.14	44:20:09.7	101.5	

Table 4—Continued

Object Number	α (J2000.0)	δ (J2000.0)	EW (\AA)	Remarks
31	20:51:03.10	44:24:03.3	...	H α ? M-star ?
32	20:51:03.68	44:24:16.1	60.4	
33N	20:50:59.00	44:19:54.9	35.6	contam. fr. nr. star
34N	20:50:59.47	44:19:39.7	72.4	
35N	20:50:48.80	44:19:23.9	16.7	
36N	20:50:46.09	44:19:10.4	8.6	
BRC 33				
1	21:34:19.65	57:30:02.6	53.4	
2	21:34:20.68	57:30:49.0	3.3	
3	21:34:49.11	57:31:25.1	66.2	very weak cont.
BRC 34				
1	21:33:29.26	58:02:50.9	43.0	weak cont.
2	21:33:55.58	58:01:18.7	...	H α ?
BRC 37				
1	21:40:25.59	56:36:38.9	...	invisible cont.
2	21:40:26.01	56:36:32.4	18.4	
3	21:40:26.80	56:36:23.8	40.9	
4	21:40:27.03	56:36:31.4	...	H α ?
5	21:40:27.37	56:36:21.9	...	M-star
6	21:40:28.08	56:36:06.1	...	invisible cont.
7	21:40:28.73	56:36:09.9	78.8	contam. fr. nr. star and bright rim
8	21:40:32.35	56:38:40.6	14.4	
BRC 38				

Table 4—Continued

Object Number	α (J2000.0)	δ (J2000.0)	EW (\AA)	Remarks
1	21:40:25.61	58:14:28.4	22.2	contam. fr. nr. star
2	21:40:27.31	58:14:21.3	59.3	contam. fr. nr. star
3	21:40:28.00	58:15:14.4	20.7	
4	21:40:31.55	58:17:55.8	...	H α ?
5	21:40:36.59	58:13:46.1	4.0	
6	21:40:36.94	58:14:38.1	63.3	
7	21:40:37.07	58:15:03.1	29.8	
8	21:40:40.35	58:13:42.9	...	H α ?
9	21:40:41.20	58:15:11.4	26.1	
10	21:40:41.59	58:14:25.8	14.8	
11	21:40:44.88	58:15:03.5	75.7	weak cont.
12	21:40:48.05	58:15:37.8	19.0	
13	21:40:48.79	58:15:00.3	...	H α ?
14	21:40:48.92	58:15:11.1	...	invisible cont., contam. fr. nr. star
15	21:40:49.11	58:17:09.4	22.2	weak cont.
16	21:41:01.81	58:15:25.4	...	H α ?
17N	21:40:38.86	58:13:03.1	100.2	
BRC 39				
1	21:45:50.30	57:26:49.7	...	H α ?
2	21:46:01.61	57:29:38.3	3.1	
3	21:46:07.12	57:26:31.6	13.0	[SII], [NII], [OI] ?
4	21:46:25.96	57:28:28.9	...	contam. fr. nr. star
5N	21:45:54.08	57:28:18.5	9.3	contam. fr. nr. star
BRC 43				
1	22:47:35.90	58:04:33.3	7.0	contam. fr. nr. stars

Table 4—Continued

Object Number	α (J2000.0)	δ (J2000.0)	EW (\AA)	Remarks
2	22:47:43.47	58:05:26.1	26.9	
3	22:47:44.57	58:03:54.3	32.7	bad pix., contam. fr. nr. sta
4	22:47:46.40	58:04:01.1	...	weak cont., contam. fr. nr. star
5	22:47:48.22	58:04:25.6	28.2	very weak cont.
6	22:47:49.29	58:04:51.1	48.6	very weak cont.
7	22:47:55.07	58:03:22.8	...	H α ?, contam. fr. nr. star
8	22:47:56.41	58:03:17.7	62.6	very weak cont., contam. fr. nr. star
9	22:48:00.24	58:02:41.8	...	contam. fr. nr. star
10	22:48:00.27	58:02:30.4	...	double star, H α /rim emission ?
11	22:48:03.73	58:05:12.3	47.7	very weak cont.
12	22:48:06.55	58:04:37.9	14.8	
13	22:48:10.46	58:04:11.4	10.8	bad pix.
14	22:48:11.53	58:03:25.0	...	H α ?
BRC 44				
1	22:28:19.01	64:13:54.0	55.8	
2	22:28:21.00	64:14:13.2	4.2	reflection nebula ?
3	22:28:41.77	64:13:11.6	...	contam. fr. nr. star
4	22:28:43.54	64:13:19.1	...	double star
5	22:28:43.98	64:13:26.0	50.6	
6	22:28:44.12	64:13:31.2	20.1	very weak cont.
7	22:28:44.74	64:13:12.0	...	contam. fr. nr. stars
8	22:28:45.31	64:13:05.6	22.5	bad pix.
9	22:28:45.48	64:13:23.0	...	contam. fr. No. 11 star
10	22:28:45.77	64:13:24.9	...	contam. fr. Nos. 5 and 12 stars
11	22:28:45.96	64:13:22.1	53.5	contam. fr. No. 9 star
12	22:28:46.24	64:13:25.6	...	contam. fr. No. 5 star
13	22:28:47.12	64:13:14.3	9.5	

Table 4—Continued

Object Number	α (J2000.0)	δ (J2000.0)	EW (\AA)	Remarks
BRC 82				
1	16:47:08.23	-41:16:08.9	29.7	
2	16:47:08.79	-41:16:15.2	7.9	
3	16:47:13.33	-41:16:39.7	...	contam. fr. nr. stars
4	16:47:14.08	-41:16:00.4	...	H α ?
5	16:47:16.51	-41:15:26.6	...	contam. fr. nr. star
6	16:47:16.50	-41:16:29.9	18.5	contam. fr. nr. star
7	16:47:18.66	-41:16:31.2	...	contam. fr. nr. stars
8	16:47:18.81	-41:16:10.3	...	H α ?
9	16:47:19.68	-41:16:14.0	15.5	contam. fr. nr. stars
10	16:47:21.70	-41:15:30.6	52.2	very weak cont., contam. fr. nr. star
11	16:47:22.94	-41:13:54.3	52.4	contam. fr. nr. star and bright rim
12	16:47:23.04	-41:15:54.5	73.6	weak cont.
13	16:47:24.08	-41:16:07.1	3.2	contam. fr. nr. star
14	16:47:24.17	-41:16:21.6	6.3	contam. fr. nr. star and bright rim
15	16:47:27.68	-41:16:29.6	158.4	contam. fr. nr. stars
16	16:47:33.28	-41:13:58.3	2.7	
BRC 89				
1	18:09:48.07	-24:06:05.6	...	H α ?
2	18:09:50.03	-24:04:36.2	...	very weak cont., contam. fr. bright rim
3	18:09:50.46	-24:05:20.3	...	H α ?
4	18:09:51.25	-24:05:51.9	75.8	
5	18:09:53.92	-24:07:31.3	18.7	contam. fr. No. 6 star
6	18:09:53.93	-24:07:32.4	...	contam. fr. No. 5 star
7	18:09:54.22	-24:06:06.1	3.6	
8	18:09:54.62	-24:06:15.9	219.4	very weak cont.
9	18:09:54.72	-24:05:43.8	46.0	

Table 4—Continued

Object Number	α (J2000.0)	δ (J2000.0)	EW (\AA)	Remarks
10	18:09:55.60	-24:06:58.0	...	contam. fr. No. 12 star
11	18:09:55.85	-24:06:09.7	71.6	contam. fr. nr. star
12	18:09:56.11	-24:06:58.5	...	contam. fr. No. 10 star
13	18:09:56.28	-24:06:48.9	25.2	contam. fr. nr. star
14	18:09:56.53	-24:06:29.8	...	contam. fr. nr. star
15	18:09:57.49	-24:06:07.1	30.1	very weak cont.
16	18:09:57.81	-24:07:16.5	91.5	weak cont.
17	18:09:57.94	-24:06:57.1	13.8	weak cont.
18	18:09:58.87	-24:06:52.7	...	contam. fr. nr. star
19	18:10:00.16	-24:07:00.3	23.9	very weak cont.
20	18:10:00.22	-24:05:19.4	21.4	
21	18:10:00.29	-24:06:28.8	7.2	
22	18:10:00.27	-24:06:51.6	59.7	very weak cont.
23	18:10:03.48	-24:07:41.6	27.7	weak cont.

S140

1	22:18:47.71	63:18:17.9	...	contam. fr. nr. stars
2	22:18:48.52	63:16:40.4	13.6	
3	22:18:49.55	63:18:56.0	...	H α ?
4	22:18:58.89	63:18:11.8	94.8	
5	22:18:59.87	63:18:52.5	...	H α ?
6	22:19:03.44	63:18:00.3	...	H α ?, contam. fr. bright rim
7	22:19:09.78	63:17:21.1	26.4	
8	22:19:16.82	63:17:22.0	163.5	very weak cont.

Cep B

1	22:56:37.97	62:39:51.1	69.7	
2	22:56:38.12	62:40:58.7	104.7	very weak cont.

Table 4—Continued

Object Number	α (J2000.0)	δ (J2000.0)	EW (\AA)	Remarks
3	22:56:39.33	62:38:15.5	80.1	
4	22:56:39.58	62:38:43.1	17.2	very weak cont.
5	22:56:39.93	62:41:37.1	14.6	M-star ?
6	22:56:43.54	62:38:07.5	...	invisible cont.
7	22:56:45.33	62:41:15.8	8.0	M-star ?
8	22:56:47.79	62:38:14.0	22.4	
9	22:56:48.02	62:38:40.2	125.6	very weak cont.
10	22:56:48.23	62:39:11.1	62.3	very weak cont.
11	22:56:49.54	62:41:10.0	21.4	
12	22:56:49.77	62:40:30.1	81.3	very weak cont.
13	22:56:51.41	62:38:55.8	...	invisible cont.
14	22:56:52.40	62:40:59.6	63.6	contam. fr. nr. star
15	22:56:53.87	62:41:17.7	19.0	
16	22:56:54.65	62:38:57.8	16.8	weak cont., contam. fr. bright rim
17	22:56:56.11	62:39:30.8	...	invisible cont.
18	22:56:57.83	62:40:14.0	59.8	
19	22:56:58.65	62:40:56.0	...	H α ?
20	22:56:59.68	62:39:20.2	76.4	
21	22:57:00.22	62:39:09.4	24.9	weak cont.
22	22:57:01.88	62:37:52.1	...	invisible cont.
23	22:57:02.63	62:41:48.7	...	contam. fr. nr. star
24	22:57:02.93	62:41:14.9	4.9	
25	22:57:04.31	62:38:21.1	...	contam. fr. neigh. stars
26	22:57:07.86	62:41:33.2	23.1	weak cont.
27	22:57:10.82	62:40:51.0	...	invisible cont., contam. fr. bright rim
28	22:57:11.48	62:38:14.1	39.6	very weak cont.
29	22:57:12.10	62:41:48.1	...	contam. fr. No. 30 star
30	22:57:13.26	62:41:49.3	...	contam. fr. No. 29 star
31	22:57:14.11	62:41:19.8	...	double star, both show H α emission
32	22:57:19.38	62:40:22.5	...	H α ?, contam. fr. bright. rim

Table 4—Continued

Object Number	α (J2000.0)	δ (J2000.0)	EW (\AA)	Remarks
33	22:57:27.04	62:41:07.9	6.4	
34N	22:57:04.93	62:38:23.2	14.2	
35N	22:57:05.91	62:38:18.4	10.1	
36N	22:56:36.14	62:36:45.9	...	invisible cont.
37N	22:56:35.29	62:39:07.8	8.1	
LW Cas				
1	02:57:03.22	60:41:39.8	14.7	
2	02:57:08.73	60:42:30.2	33.9	weak cont.
3	02:57:13.80	60:40:59.3	30.8	
4	02:57:15.70	60:38:49.3	...	M-star ?
5	02:57:20.82	60:41:27.4	55.4	very weak cont.
6	02:57:27.08	60:41:51.4	8.2	contam. fr. No. 7 star
7	02:57:28.11	60:41:49.2	36.0	contam. fr. No. 6 star
8	02:57:28.34	60:42:33.0	...	H α ?
9	02:57:29.53	60:42:28.1	...	double star
10	02:57:32.81	60:41:29.7	48.6	very weak cont.
11	02:57:37.67	60:39:58.6	...	invisible cont.
12	02:57:40.53	60:39:07.5	9.9	very weak cont.
13N	02:57:51.23	60:40:00.9	53.7	very weak cont.
Ori I-2N				
1	05:37:51.12	-1:36:17.0	...	H α ?, weak cont.
2	05:37:59.11	-1:36:56.3	7.0	
3	05:38:02.32	-1:36:34.4	...	H α ?, weak cont.
4	05:38:02.58	-1:34:39.5	...	M-star ?
5N	05:37:51.41	-1:36:42.3	6.7	

